THE PROPERTIES OF GALAXIES IN X-RAY BRIGHT AND FAINT GROUPS

THE PROPERTIES OF GALAXIES IN X-RAY BRIGHT AND FAINT GROUPS

By

ADAM ROYLE, B.Sc., M.Sc.

A Thesis
Submitted to the School of Graduate Studies
in Partial Fulfillment of the Requirements
for the Degree
Master of Science

McMaster University

MASTER OF SCIENCE (2014) McMaster University
(Physics and Astronomy) Hamilton, Ontario

TITLE: The Properties of Galaxies in X-ray Bright and Faint Groups

AUTHOR: Adam Royle, B.Sc., M.Sc.(Memorial University of Newfoundland)

SUPERVISOR: Laura Parker

NUMBER OF PAGES: x, 82

Abstract

Galaxy groups are an intermediate density environment in which more than half of the galaxies in the local universe reside. Galaxy groups have a small contrast against the vast background of galaxies and therefore until recently it has remained very difficult to identify large samples. Using observational data from the Group Environment and Evolution Collaboration (GEEC) and the Cosmological Evolution Survey (COSMOS) new calculations of passive fractions and disk fractions for galaxies in X-ray bright and faint groups are investigated. How these fractions depend on the overall environment, galaxy stellar mass, total group mass, group-centric distance, group X-ray luminosity and redshift is examined. It was found that the passive and disk fractions were different in X-ray bright and faint groups and depend most strongly on galaxy stellar mass, redshift and overall environment with less dependence on the other parameters. Attempts to connect the star formation and morphology results are made.

The results show that the passive fractions were higher in X-ray groups yet the disk fractions were also found to be higher in these groups. This was a surprising result as disk-like galaxies are typically associated with star-forming galaxies. The results show the complexity within galaxy groups.

Acknowledgements

Thank you to my supervisor Laura Parker for her patience, help and guidance over the past two years.

Thank you to my committee members Alison Sills and Christine Wilson. Thank you to the staff in the Department of Physics and Astronomy at McMaster University. Thank you to all of my professors, past and present, especially John Lewis and thank you to all my classmates, group members and friends.

Last but certainly not least, thank you to my parents and family for their support and encouragement.

Contents

List of Figures

List of Tables

Chapter 1

Introduction

Galaxies are found in a variety of environments, ranging from isolated field galaxies to groups and clusters and the properties of galaxies are strongly dependent on the environment in which they are found. Galaxy groups are a very active area of research for a number of reasons: they are the most common environment in which galaxies reside in the local universe (Eke et al., 2004), groups are an intermediate environment between the field and galaxy clusters (Wilman et al., 2005) and in fact our own galaxy, the Milky Way, is part of a small group. They play a vital role in understanding the effects of environment on galaxy evolution as with smaller velocity dispersions in comparison to clusters (Barnes, 1985), there are many more galaxy-galaxy interactions and as a result it is in groups where many galaxy transformation processes have been found to be the most efficient (Zabludoff & Mulchaey, 1998; Balogh et al., 2011).

Groups generally have between 3-50 members and velocity dispersions in the range 200-800 km/s (systems with membership and velocity dispersions greater than this are generally called clusters). Group masses generally range from about 10^{12}-10^{14} $M_{\odot}$ with virial radii approximately 200-1000 kpc (Connelly et al., 2012). While the Local Group is a special type of small group which we are able to detect due to its proximity, detection of groups at higher redshifts is much more difficult in part due to their small contrast with respect to the vast background of galaxies. With improved

group finding methods such as the Friends-of-Friends algorithm (Huchra & Geller, 1982), which links galaxies in projected position and redshift space, it is now possible to obtain sizable samples.

Groups are generally divided into two main types: compact and loose (Helsdon & Ponman, 2000). Each type has a unique set of properties with compact groups being those where the distance between galaxies is comparable to the sizes of the galaxies themselves, for example the Hickson Compact Groups (Hickson, 1982) and Stephan's Quintet, as shown in the HST image in Figure 1.1. The middle of the image shows two merging galaxies and the upper left of the image shows a tidally disrupted galaxy. Different groups have galaxies undergoing different processes and active vs relaxed systems will undoubtedly shape the galaxy morphologies and overall properties. Compact groups may evolve into fossil groups where all members eventually merge into one large galaxy with some satellites (e.g. Miller et al., 2012).

Figure 1.1: Stephan's Quintet galaxy group. Interacting galaxies are present with a merging pair at centre and a tidally disruptive galaxy at the upper left. Image credit: NASA. `http://www.nasa.gov/mission_pages/hubble/hubble_anniversary/STScI-2009-25c.html`

On the other hand, the separation between galaxies in loose groups is much larger and loose groups may grow over time and become cluster-like. Loose groups can range from systems like the Local Group which contains two bright dominant galaxies, the Milky Way and Andromeda, along with a number of satellite galaxies (as shown in Figure 1.2) to much larger systems. Loose groups will be the focus of this thesis and there are now a number of large catalogs of loose groups such as: the Group Environment and Evolution Collaboration (GEEC) (Carlberg et al., 2001; Wilman et al., 2005), the Cosmological Evolution Survey (COSMOS) (Scoville et al., 2007) and the Sloan Digital Sky Survey (SDSS) (York et al., 2000).

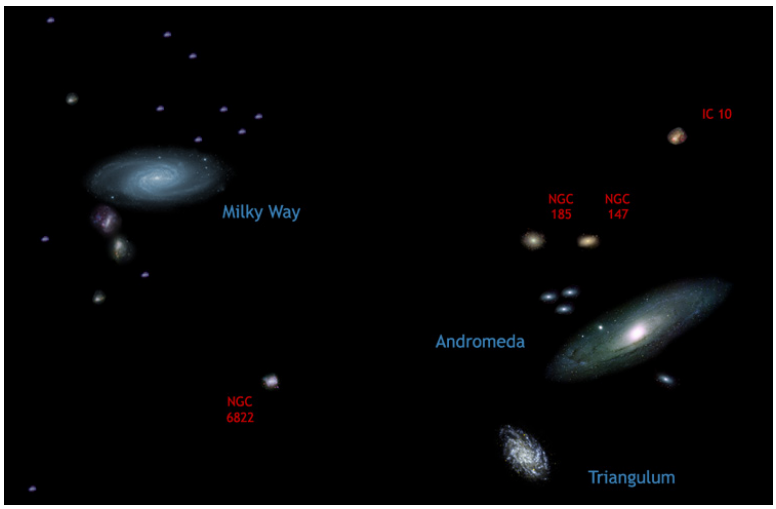

Figure 1.2: A schematic of the Local Group of galaxies. Two dominant spirals, the Milky Way and Andromeda, along with a number of satellite galaxies comprise the group. The Local Group is a small group which we are able to detect due to its proximity. Image credit: Dronaias.com. `http://dronaias.com/galaxy/`

Figure 1.3 shows images of two loose GEEC groups taken with the Hubble Space Telescope both at a redshift of approximately 0.4 and both with velocity dispersions of ∼230 km/s. The left is an elliptical/S0-dominated group while the right image is a spiral-dominated group. It is interesting to note that groups with similar overall properties can contain galaxies of different morphologies as these images show.

With the GEEC and COSMOS samples (to be described in Chapter 2), the prop-

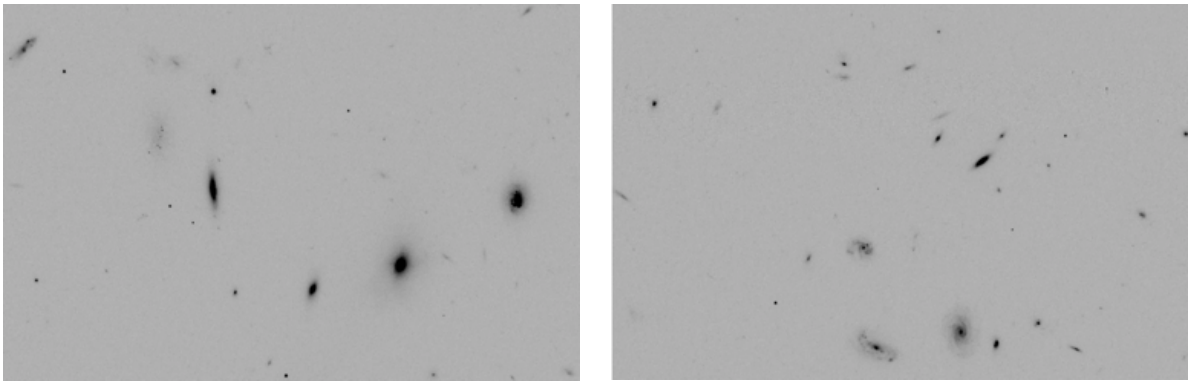

Figure 1.3: Hubble Space Telescope images of two GEEC groups both at a redshift ∼0.4 and with velocity dispersions of ∼230 km/s. The left is an elliptical/S0-dominated group while the right image is a spiral-dominated group. These two groups clearly show the diversity in group galaxy member properties, despite the two groups having nearly identical overall properties such as their masses and redshifts.

erties of galaxies in groups can be investigated in detail. How the properties depend on overall environment, group mass, group-centric distance, X-ray luminosity and redshift will be explored. As will be shown below, some of these trends and relations have been confirmed for galaxy properties on the cluster scale but are still a matter of debate on the group scale.

1.1 Environmental Dependencies

1.1.1 Star Formation

The environment in which a galaxy is found is vital in understanding its properties and subsequent evolution. Different processes are known to occur in different environments and as mentioned, groups are the most efficient environment in which some of these processes take place (Barnes, 1985; Zabludoff & Mulchaey, 1998; Balogh et al., 2011). The work of Rawle et al. (2014) also suggests the pre-processing of galaxies in groups before they encounter the cluster environment (i.e. galaxy evolution takes place at the group scale before the galaxies become part of a cluster). They studied

clusters at similar stages in their merger processes and with similar properties such as redshift and overall galaxy density. However, the galaxies in the clusters show differences in their star formation rates (and other properties such as dust temperature) suggesting that the galaxy properties are not a direct result of the recent cluster mergers but instead are likely the imprints of the groups which combined to form the cluster.

One property of a galaxy that has been shown to depend strongly on environment is its star formation rate. Figure 1.4 shows the dominant star formation quenching mechanisms for galaxies as a function of stellar mass and redshift as adapted from Peng et al. (2010) (see their Figure 15). For higher mass galaxies, the dominant quenching mechanism is due to internal processes. Perhaps these high mass galaxies contain supermassive black holes at their centres which act to heat the surrounding gas thus not allowing the cooling of the gas to form stars. For lower mass galaxies the external environment plays a more vital role. At high redshifts, the dominant quenching mechanism for low mass galaxies is merging. As the merger rate was higher in the past, mergers may act to suppress the star formation of the galaxies (after the initial starburst phase produced by the merger, e.g. Mihos & Hernquist, 1996; Urquhart et al., 2010). At lower redshift and when the merger rate is much lower the dominant mechanism is environment quenching. This environment quenching can take on many forms, for example ram pressure stripping (where cold gas is stripped from the galaxy) (Abadi, Moore & Bower, 1999) and/or strangulation (where the hot gas is removed from the galaxy diminishing the future cold gas supply) (Kawata & Mulchaey, 2008). Thus in short, overall environment plays a more important role in quenching star formation for low mass galaxies whereas for higher mass galaxies internal processes regulate star formation and these internal processes are the more efficient quenching mechanism.

To further show the influence environment has on galaxy properties, Figure 1.5 shows the fraction of star-forming galaxies as a function of redshift for field, low mass

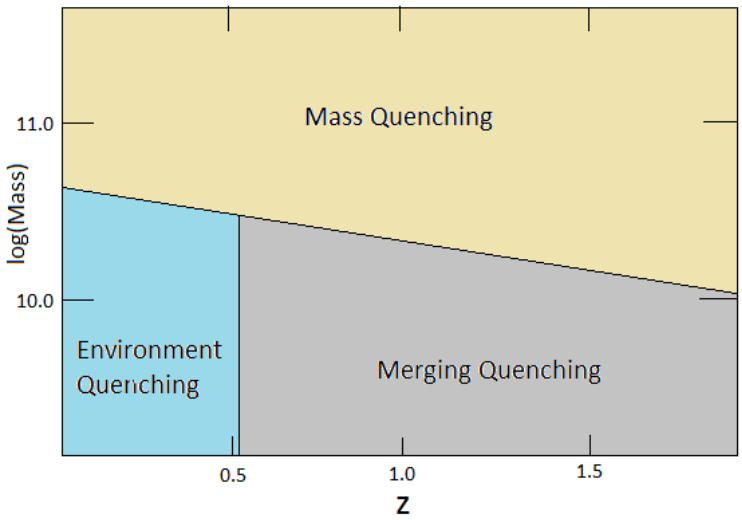

Figure 1.4: The dominant star formation quenching mechanisms as a function of galaxy stellar mass and redshift as adapted from Peng et al. (2010) (see their Figure 15). Environment plays a major role for low mass galaxies while intrinsic processes are the dominant quenching mechanisms for high mass galaxies.

groups, high mass groups and clusters (the green points) as measured by Giodini et al. (2012) (see their Figure 8). First of all Figure 1.5 shows that the amount of star formation increases as a function of redshift in all environments. At higher redshift there is a higher amount of gas to be exhausted. The figure also shows that at any particular redshift there is more star formation ongoing in the field compared to groups and in groups compared to the clusters. Thus, as the structure in which galaxies are found becomes larger the overall amount of star formation decreases. This again is likely a result of environmental processes such as ram pressure stripping (Abadi, Moore & Bower, 1999) and/or strangulation (Kawata & Mulchaey, 2008).

1.1.2 Morphology

Another property of a galaxy that is dependent on environment is its morphology. It has been shown that the proportion of spiral galaxies declines in high density environments while the fraction of ellipticals and S0 galaxies increases as density

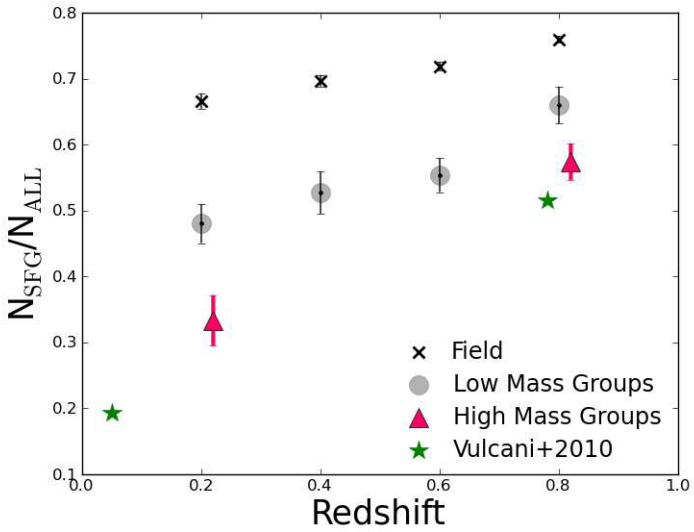

Figure 1.5: The fraction of star-forming galaxies as a function of redshift for field, low mass groups, high mass groups and cluster galaxies (the green points). Larger scale structures such as groups and clusters quench star formation more so than the field. Image credit: Giodini et al. (2012) (see their Figure 8). Reproduced with permission © ESO.

increases (Dressler, 1980). For example, Butcher & Oemler (1978) concluded that the high density centres of clusters typically contain red, non-star-forming ellipticals while the less dense outer regions typically contain blue, star-forming spirals. The morphology-density relation has since been confirmed by others (e.g. Dressler et al., 1997; Treu et al., 2003). Their results also show that the fraction of elliptical galaxies typically increases from the field to groups to clusters. Figure 1.6 summarizes the morphology-density relation. The figure shows the fractions of spiral, S0 and elliptical galaxies as a function of galaxy density (in units of the number of galaxies per cubic megaparsec), with the density of galaxies increasing from the field (isolated galaxies) to groups to clusters. The fraction of elliptical and S0 galaxies increase as a function of density while the spiral fraction decreases as a function of density. It should be noted as well that the overall spiral fraction has been shown to increase with redshift (Butcher & Oemler, 1978).

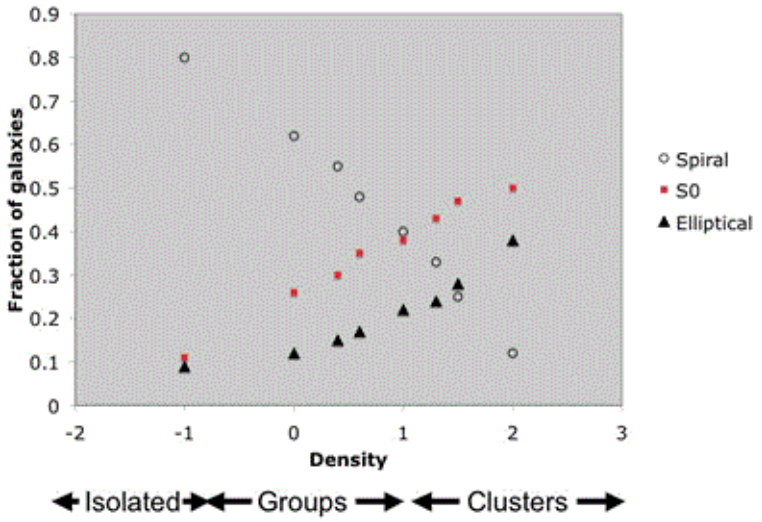

Figure 1.6: Morphology-density relation showing the fractions of spiral, S0 and elliptical galaxies as a function of galaxy density (in units of the number of galaxies per cubic megaparsec), with the density of galaxies increasing from the field (isolated galaxies) to groups to clusters. The fraction of elliptical and S0 galaxies increases as a function of density while the spiral fraction decreases as a function of density. Image credit: Swinburne University of Technology. `http://astronomy.swin.edu.au/cosmos/M/Morphology+Density+Relation`

1.2 Halo Mass Dependencies

How the properties of galaxies depend on the total halo mass of the groups in which they reside is also an active topic of research. Figure 1.7 shows the quiescent (i.e. passive or non-star-forming) fraction, f_q, for galaxies within $2r_{200}$ (r_{200} being the radius of the group within which the average density is 200 times the critical density of the universe, giving a measure of the virial radii of the groups) as a function of redshift as measured by Hou et al. (2013) (see their Figure 4). The work presented in Figure 1.7 uses a combination of data from the Group Environment and Evolution Collaboration (GEEC) (Wilman et al., 2005; Connelly et al., 2012), GEEC2 (Balogh et al., 2011) and the Sloan Digital Sky Survey (SDSS) (McGee et al., 2011) for various stellar mass galaxy bins and subdivided into low mass (circles) and high mass (triangles) groups and M_{200} represents the group dynamical mass which is described further in Section

2.1. No clear dependence on group mass is observed as most of the points tend to overlap within error and neither the low or high mass groups produce systematically higher or lower quiescent fractions.

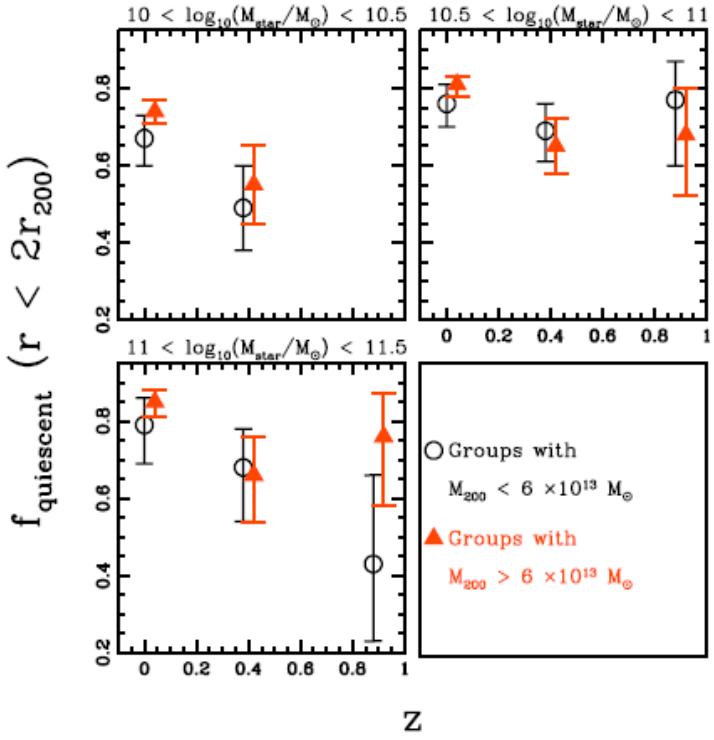

Figure 1.7: Quiescent fraction within $2r_{200}$ as a function of redshift for various stellar mass galaxy bins subdivided into galaxies found in low mass (circles) and high mass (triangles) groups. No clear dependence on group mass is observed as the points tend to overlap in all panels. Image credit: Hou et al. (2013) (see their Figure 4). © MNRAS

The results of Giodini et al. (2012) from Figure 1.5 however do suggest a halo mass dependence. The result there showed that galaxies in higher mass groups have a lower star-forming fraction than the low mass groups. Wetzel, Tinker & Conroy (2012) used SDSS data and also observed a lower fraction of star-forming galaxies as a function of increasing halo mass. In terms of morphology, it is still in debate whether or not spiral fractions depend on group and/or cluster mass (or X-ray luminosity, as discussed below in Section 1.4) (Poggianti et al., 2009). Thus, halo mass dependencies

in groups are still a matter of debate and will be investigated in this thesis.

1.3 Radial Dependencies

Radial trends have been observed in clusters with red, non-star-forming galaxies typically found near the cluster centres (Butcher & Oemler, 1978; Dressler, 1980) but the existence of radial trends in groups are not as clear (Ziparo et al., 2013). Figure 1.8 shows the red fraction as a function of redshift for cluster galaxies in various radial bins as measured by Loh et al. (2008) (see their Figure 6). The red fraction is anti-correlated with star formation and so as the red fraction decreases the amount of star formation increases. The figure divides the galaxies into radial bins as indicated with the radii normalized by the cluster r_{200}. The results show that at any particular redshift as you move from the inner part of the cluster towards the outer regions the red fraction decreases and thus the amount of star formation increases. The red fraction results here also suggest more star formation at higher redshift as was also observed in Figure 1.5 and as expected from the Butcher-Oemler effect originally presented by Butcher & Oemler (1978) and since confirmed in a number of studies of clusters (e.g. Nilo Castellón et al., 2014).

Figure 1.8 confirms that radial trends have been observed in clusters but as mentioned, the trends are still a matter of debate in groups. Ziparo et al. (2013) find a lack of star formation gradients while Rasmussen et al. (2012) and Wetzel, Tinker & Conroy (2012) observe radial trends, with the star formation decreasing near the centres of halos. However, careful comparisons between analyses are required. For example, some papers may use optically selected groups while others use X-ray selected. Some studies only observe as far as the virial radius while others may extend to two or three virial radii which may make the trends more obvious. Other studies may use photometric redshifts which increases the error and thus raise the chances of incorrectly identifying interlopers as group members while others may use spec-

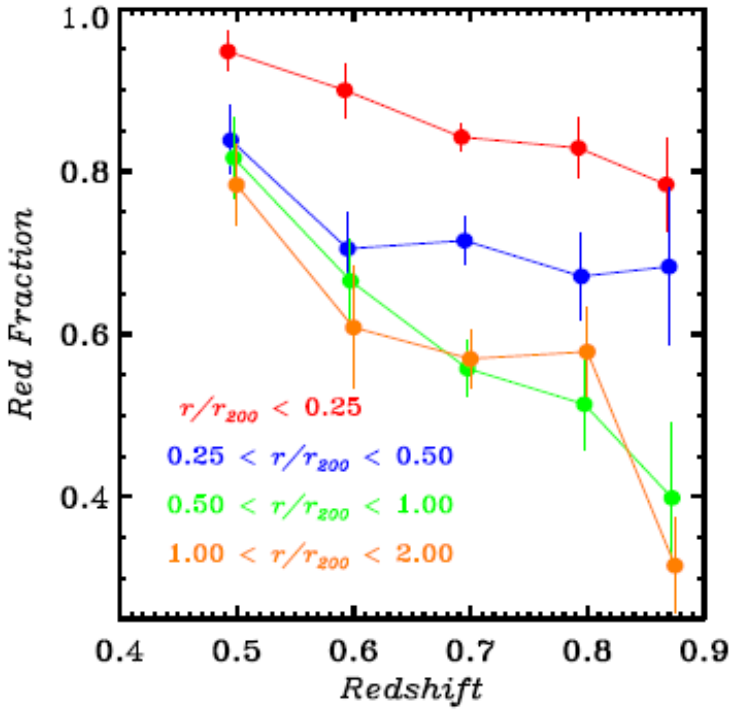

Figure 1.8: Red fraction (which is anti-correlated with star formation) as a function of redshift for cluster galaxies in various cluster-centric bins. Galaxies near the centre have redder colours compared to galaxies found in the outer regions of the cluster. Image credit: Loh et al. (2008) (see their Figure 6). © AAS. Reproduced with permission.

troscopic redshifts with smaller uncertainties. Making sure the galaxies have similar stellar mass distributions (to be discussed in more detail in Chapter 2) is also critical. These considerations can all affect the results and thus a more detailed and proper comparison into seemingly contradictory results is necessary.

1.4 X-ray Luminosity

Galaxy groups themselves show diversity and can be subdivided into X-ray bright and X-ray faint groups. X-ray faint groups can be located in the optical by finding galaxies that are close in projection and in redshift space. The X-ray measurements have been

made in recent years (Finoguenov et al., 2007, 2009) with the X-ray emission tracing the hot gas of the intra-group medium (IGM). These groups are found by observing the extended X-ray emission and then searching for galaxies that are grouped together in the overlapping redshift and position space around this emission (Erfanianfar et al., 2013). So, the X-ray luminous groups (hereafter referred to as the X-ray groups) with extended X-ray emission also have optical members which can be confirmed spectroscopically. In general, higher X-ray flux is found for higher mass systems. However, several X-ray faint groups (hereafter referred to as optical groups) possess similar masses to some of the X-ray luminous groups suggesting another parameter must be considered to explain the scatter. This thesis looks at trends with X-ray luminosity to try and understand how the properties of galaxies in groups depend on X-ray luminosity.

Some work has been completed comparing the X-ray and optical systems. Figure 1.9 taken from Connelly et al. (2012) (see their Figure 14) shows the $M_{stellar}$-L_x and $M_{dynamical}$-L_x relations for X-ray and optical systems where $M_{stellar}$ is the total stellar mass of the group (corrected to include low mass galaxies that may have gone undetected) and $M_{dynamical}$ is a measure of the total group mass. The colour scheme is described in Connelly et al. (2012) but for our purposes here, the main point is that relatively tight relationships are observed but with several outliers and some scatter. Attempting to understand the scatter and outlier points by studying the individual galaxy properties within the groups will help ascertain the differences between the X-ray and optical systems. While the properties and scaling relations for the X-ray and optical groups as a whole have been studied, this thesis is the first known work undergoing an in-depth analysis comparing the properties of member galaxies between these two types of groups.

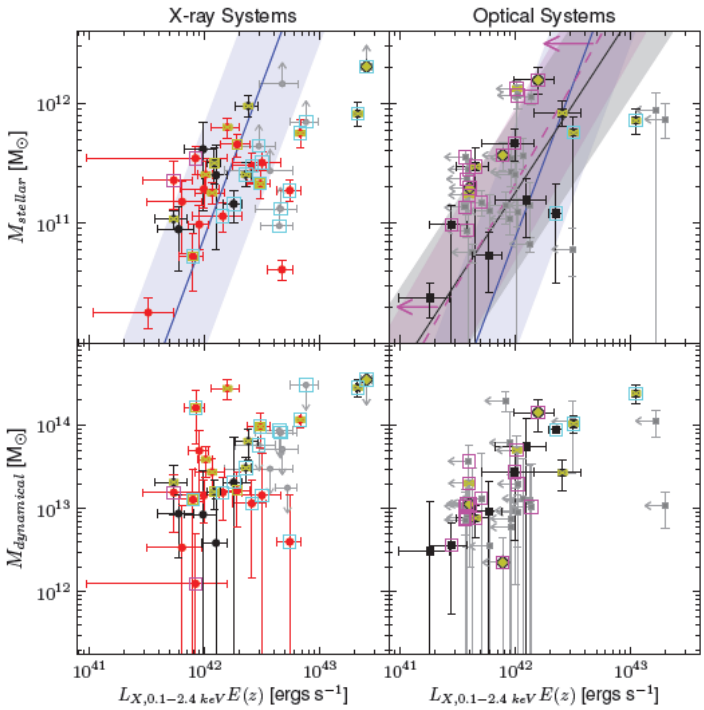

Figure 1.9: $M_{stellar}$-L_x and $M_{dynamical}$-L_x relations for X-ray and optical systems. The colour scheme is as described in Connelly et al. (2012). Overall, tight relationships are found but scatter is observed as outliers are present. Trying to understand these outliers is an active topic of research. Image credit: Connelly et al. (2012) (see their Figure 14). © AAS. Reproduced with permission.

1.5 Thesis Objectives

The goal of this thesis is to compare the star formation and morphology properties for galaxies in X-ray and optical groups. Specifically, how these properties depend on overall environment, group mass, group-centric distance, X-ray luminosity and redshift is investigated. Chapter 2 introduces the galaxy and group samples. Chapters 3 and 4 show the passive fraction results obtained from the Group Environment and Evolution Collaboration (GEEC) data and the disk fraction results obtained from the Cosmological Evolution Survey (COSMOS) respectively while Chapter 5 discusses and summarizes the results and suggests future directions of work.

We focus on passive fractions in GEEC because of good SFR measurements and a lack of HST morphology measurements and we focus on disk fractions in COSMOS because of excellent HST morphology measurements while there were no SFR catalogs publicly accessible. As has been discussed above, some trends in galaxy properties have been observed in clusters but are still debatable at the group scale. This thesis investigates these trends on the group scale.

Bibliography

Abadi, M. G., Moore, B., & Bower, R. G., 1999, MNRAS, 308, 947

Balogh, M. L., McGee, S. L., Wilman, D. J., et al., 2011, MNRAS, 412, 2303

Barnes, J., 1985, MNRAS, 215, 517

Butcher, H. & Oemler Jr., A., 1978, ApJ, 219, 18

Carlberg, R. G., Yee, H. K. C., Morris, S. L., et al., 2001, ApJ, 552, 427

Connelly, J. L., Wilman, D. J., Finoguenov, A., et al., 2012, ApJ, 756, 139

Dressler, A., 1980, ApJ, 236, 315

Dressler, A., Oemler Jr., A., Couch, W. J., et al., 1997, ApJ, 490, 577

Eke, V. R., Baugh, C. M., Cole, S., et al., 2004, MNRAS, 348, 866

Erfanianfar, G., Finoguenov, A., Tanaka, M., et al., 2013, ApJ, 765, 117

Finoguenov, A., Guzzo, L., Hasinger, G., et al., 2007, ApJS, 172, 182

Finoguenov, A., Connelly, J. L., Parker, L. C., et al., 2009, ApJ, 704, 564

Giodini, S., Finoguenov, A., Pierini, D., et al., 2012, A&A, 538, A104

Helsdon, S. F. & Ponman, T. J., 2000, MNRAS, 319, 933

Hickson, P., 1982, ApJ, 255, 382

Hou, A., Parker, L. C., Balogh, M. L., et al., 2013, MNRAS, 435, 1715

Huchra, J. P. & Geller, M. J., 1982, ApJ, 257, 324

Kawata, D. & Mulchaey, J. S., 2008, ApJ, 672, L103

Loh, Y.-S., Ellingson, E., Yee, H. K. C., et al., 2008, ApJ, 680, 214

McGee, S. L., Balogh, M. L., Wilman, D. J., et al., 2011, MNRAS, 413, 996

Mihos, J. C. & Hernquist, L., 1996, ApJ, 464, 641

Miller, E. D., Rykoff, E. S., Dupke, R. A., et al., 2012, ApJ, 747, 94

Nilo Castellón, J. L., Alonso, M. V., García Lambas, D., et al., 2014, MNRAS, 437, 2607

Peng, Y.-j., Lilly, S. J., Kovač, K., et al., 2010, ApJ, 721, 193

Poggianti, B. M., Fasano, G., Bettoni, D., et al., 2009, ApJL, 697, L137

Rasmussen, J., Mulchaey, J. S., Bai, L., et al., 2012, ApJ, 757, 122

Rawle, T. D., Altieri, B., Egami, E., et al., 2014, MNRAS, 442, 196

Scoville, N., Aussel, H., Brusa, M., et al., 2007, ApJS, 172, 1

Treu, T., Ellis, R. S., Kneib, J-P., et al., 2003, ApJ, 591, 53

Urquhart, S. A., Willis, J. P., Hoekstra, H., et al., 2010, MNRAS, 406, 368

Wetzel, A. R., Tinker, J. L. & Conroy, C., 2012, MNRAS, 424, 232

Wilman, D. J., Balogh, M. L., Bower, R. G., et al., 2005, MNRAS, 358, 71

York, D. G., Adelman, J., Anderson Jr., J. E., et al., 2000, AJ, 120, 1579

Zabludoff, A. I. & Mulchaey, J. S., 1998, ApJ, 496, 39

Ziparo, F., Popesso, P., Biviano, A., et al., 2013, MNRAS, 434, 3089

Chapter 2

Data

Two major surveys were utilized in this thesis, the Group Environment and Evolution Collaboration (GEEC) survey and the Cosmological Evolution Survey (COSMOS). The multi-wavelength data set of GEEC has excellent SED measurements allowing for good star formation rate and stellar mass estimates, while the COSMOS survey had extensive HST coverage allowing for very good morphology measurements. COSMOS also has extensive multi-wavelength coverage but SFR data was not publicly available.

2.1 GEEC

The Group Environment and Evolution Collaboration (GEEC) survey (Wilman et al., 2005) is an extension of the Canadian Network for Observational Cosmology 2 survey (CNOC2) (Carlberg et al., 2001; Yee et al., 2000) which covered four patches of the sky totaling an area of approximately 1.5 deg^2 and covering a redshift range from $\sim$0.1-0.6. GEEC performed extensive multi-wavelength follow-up including X-ray observations of two of the fields (Finoguenov et al., 2009; Connelly et al., 2012). There were a total of approximately 200 spectroscopically confirmed groups (Wilman et al., 2005). The spectroscopic redshifts allowed for confidence in the group finding as opposed to solely using photometric redshifts which have much higher error and

thus a greater chance of incorrectly identifying interloper foreground and background galaxies as group members. For this particular study approximately 70 X-ray and 80 optically selected groups with spectroscopic data with approximately 3800 field, 500 X-ray and 500 optical group galaxies respectively were used from the catalogs of Connelly et al. (2012). Data was obtained from the infrared to the X-ray using such instruments as GALEX, the Hubble Space Telescope, Spitzer, XMM-Newton and Chandra with spectroscopy from CFHT, Magellan, Gemini and the VLT (Very Large Telescope) (Connelly et al., 2012).

Figure 2.1 shows the distributions of the group redshift (left), mass (right) and X-ray luminosity (bottom) for the X-ray and optical groups (with the X-ray luminosity data for the X-ray groups only). The group (or halo) mass here comes from the dynamical mass estimate of the group which is found from the group velocity dispersion through the relation

$$M_{dyn} = \frac{3r_{200}\sigma^2}{G} \tag{2.1}$$

where σ is the velocity dispersion of the group, G is the gravitational constant and r_{200} again is the radius of the group inside of which the average density is 200 times the critical density of the universe and gives an estimate of the virial radius of the group. Since groups have different sizes, r_{200} serves to normalize the groups to a common radius to allow for a proper comparison between the groups. It is found from the relation

$$r_{200} = \frac{\sigma\sqrt{3}}{10H(z)} \tag{2.2}$$

where $H(z) = H_o\sqrt{\Omega_M(1+z)^3 + \Omega_k(1+z)^2 + \Omega_\Lambda}$ where H_o is the Hubble constant, z is the redshift of the group and Ω_M, Ω_k and Ω_Λ are the dimensionless density parameters (Hogg, 1999). Throughout this thesis we assume a cosmology $H_o = 70$ km s^{-1} Mpc^{-1}, $\Omega_M = 0.3$, $\Omega_k = 0$ and $\Omega_\Lambda = 0.7$.

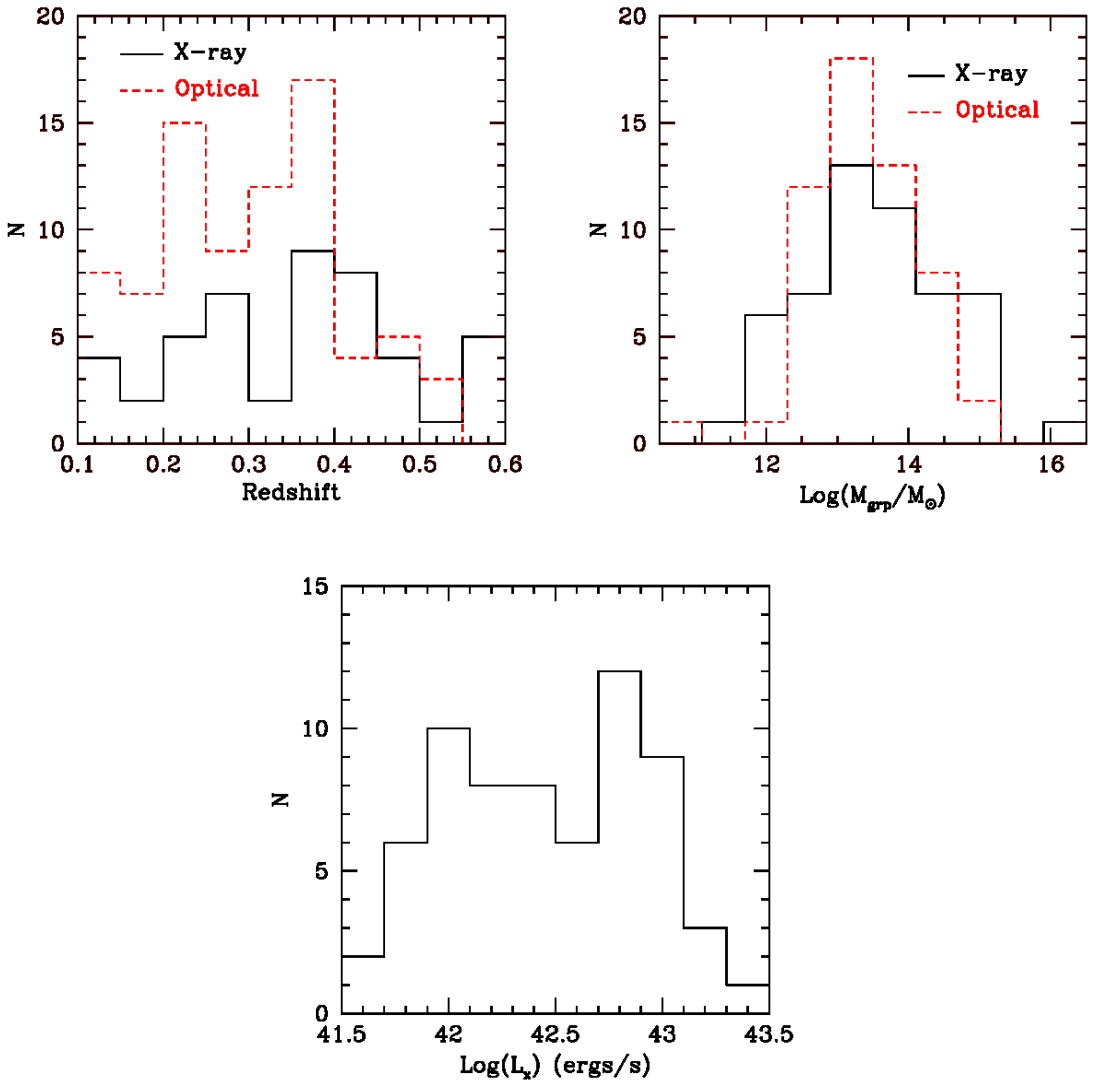

Figure 2.1: Distribution of redshifts (left), total stellar mass (right) and X-ray luminosity (bottom) for the X-ray and optical GEEC groups. Only X-ray groups are included in the bottom panel.

The redshifts cover a similar range among the two types of groups with a range ∼0.1-0.6. It should be noted that the X-ray groups have been detected to a redshift of approximately 1 but star formation data was only available to a redshift of approximately 0.6 and hence the X-ray sample was only studied up to this redshift (which allowed for direct comparison to the optical sample). The group mass also follows a similar range of values between both types of groups with the X-ray groups slightly more massive while the X-ray luminosities cover a range of approximately 41.5<log(L_x) (erg/s)<43.5.

Figure 2.2 shows the redshift (left), stellar mass (right) and specific star formation rates (bottom) for field, X-ray and optical group galaxies. Since the field galaxy sample was much larger than the X-ray and optical group galaxy samples, the fraction of galaxies was plotted rather than the raw number, in order to allow for a comparison with the group samples. The stellar masses and star formation rates were obtained from Spectral Energy Distribution (SED) fits from the IR to UV (McGee et al., 2011). The specific star formation rate (sSFR) quantifies the efficiency of star formation and is the star formation rate (SFR) in solar masses per year divided by the total stellar mass of the galaxy (in units of solar mass). That is,

$$sSFR = \frac{SFR(M_{\odot}yr^{-1})}{M_{*}(M_{\odot})} \tag{2.3}$$

Galaxies with sSFR>10^{-11} yr^{-1} are considered star-forming while those with sSFR<10^{-11} yr^{-1} are non-star-forming. This cut comes from the bimodality of the sSFR distribution as can be seen in the bottom panel of Figure 2.2 with the minimum of the distribution at approximately log(sSFR) = -11 yr^{-1}. The sSFR panel of Figure 2.2 clearly shows that field galaxies have a higher fraction of star-forming galaxies than the groups.

This division between star-forming and non-star-forming galaxies can also be seen in Figure 2.3 as measured in McGee et al. (2011) (see their Figure 5) which shows the distribution of field and group galaxies in the sSFR-stellar mass plane taken from

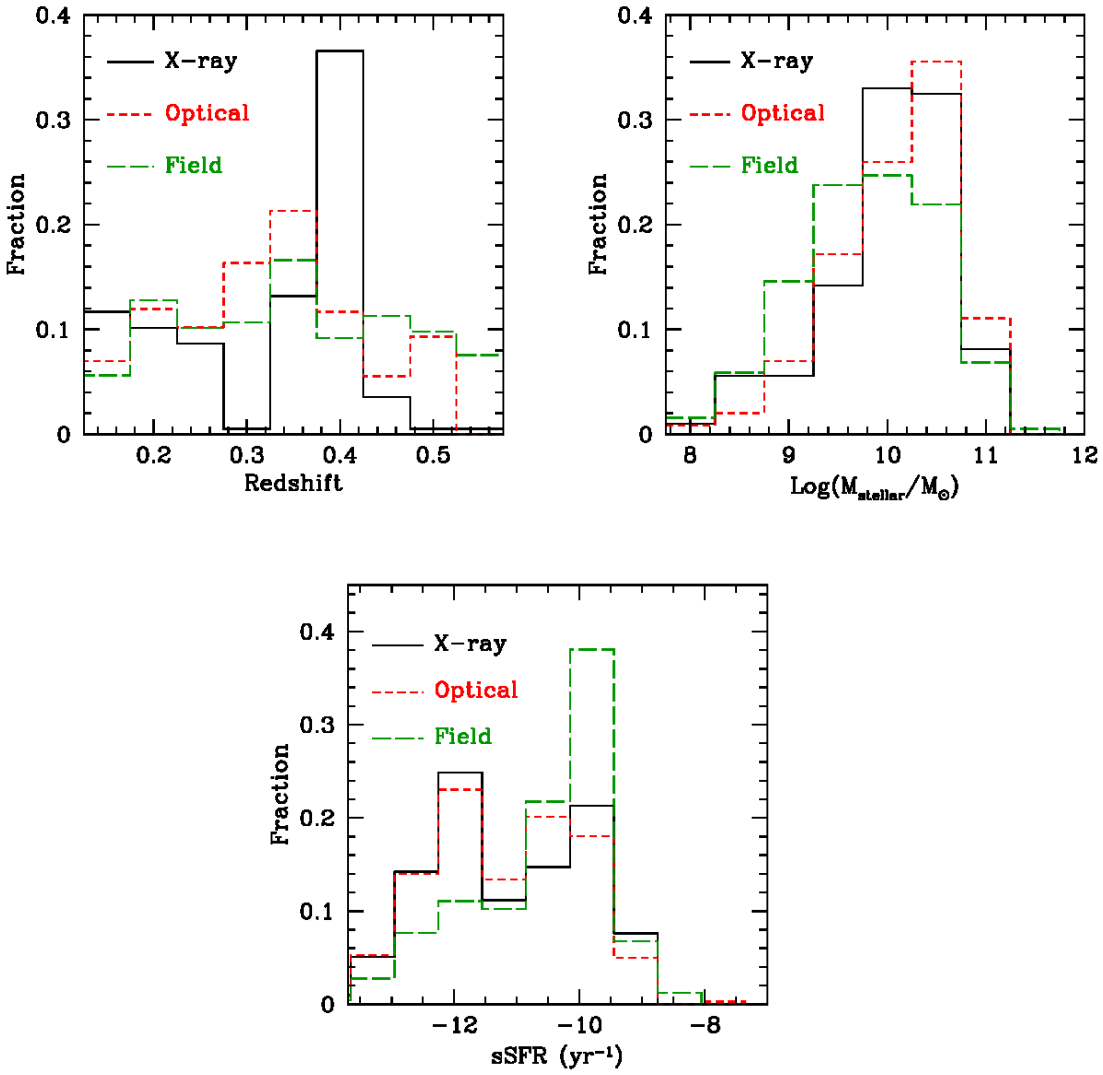

Figure 2.2: Distributions of redshift (left), stellar mass (right) and sSFR (bottom) for GEEC galaxies in the field and in X-ray and optical groups.

SDSS data at a median redshift of approximately 0.08. The dashed red line represents log(sSFR) = -11 yr^{-1}. Two overdensities of galaxies are observed in both panels. The higher sSFR overdensity contains an abundance of low mass galaxies while the low sSFR overdensity contains mostly high stellar mass galaxies with the dashed line representative of the split between the two populations. Thus, the figure shows that high mass galaxies are typically passive while low mass galaxies are typically more star-forming as especially evident in their field sample.

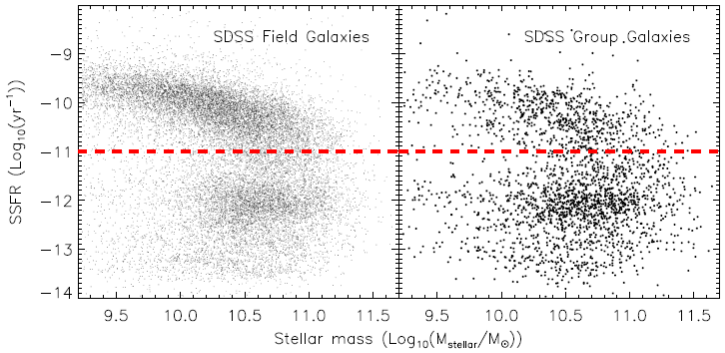

Figure 2.3: The distribution of field and group galaxies in the sSFR-stellar mass plane taken from the SDSS survey with median redshift 0.08. The dashed red line represents log(sSFR) of -11 yr^{-1} with galaxies above this line considered star-forming while those below are considered non-star-forming galaxies. Note that star-forming galaxies are typically low mass while non-star-forming galaxies are typically more massive. Image credit: McGee et al. (2011) (see their Figure 5). © MNRAS

Before analyzing the data in detail, stellar mass incompleteness needs to be considered. There are many more low mass galaxies in the universe and so mass functions showing stellar mass distributions are expected to continuously increase from the high mass to low mass end. However, these low mass galaxies are much harder to detect, especially at higher redshift, and so a turnoff is observed in these histograms, as illustrated in Figure 2.4 which shows the stellar mass distribution for the entire GEEC sample. Samples of galaxies with masses greater than the turnoff are considered complete while samples of galaxies with masses below this turnoff are stellar mass

incomplete.

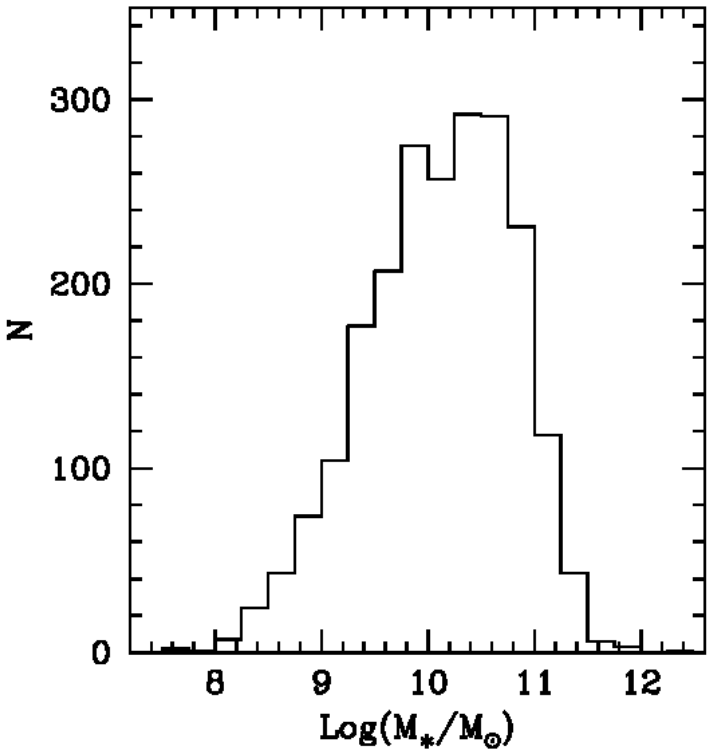

Figure 2.4: The stellar mass distribution of the GEEC galaxies. The turnover suggests a stellar mass completeness limit of $10^{10.2} M_{\odot}$ for the entire GEEC sample.

From Figure 2.4 showing the stellar mass distribution of the GEEC sample, the stellar mass cutoff is approximately $10^{10.2} M_{\odot}$. This figure represents the entire GEEC sample. In order to be able to include lower mass galaxies, the galaxies were divided into redshift bins of 0-0.2, 0.2-0.4 and 0.4-0.6. Finding the turnover of the mass distributions for each of these individual redshift bins produces different cutoffs as a function of the redshift allowing lower mass galaxies to be included in the analysis at the lower redshifts and avoids diminishing the sample size too significantly. Figure 2.5 shows this stellar mass cutoff as a function of redshift. The redshift value represents the median redshift of the galaxies in each of the three redshift bins 0-0.2, 0.2-0.4 and 0.4-0.6. Thus looking at the figure, galaxies at a redshift of approximately 0.48,

for example, are complete to approximately $10^{10.7} M_{\odot}$ and so only those galaxies with stellar masses greater than this cutoff at this redshift are included in the analysis creating a stellar mass complete sample.

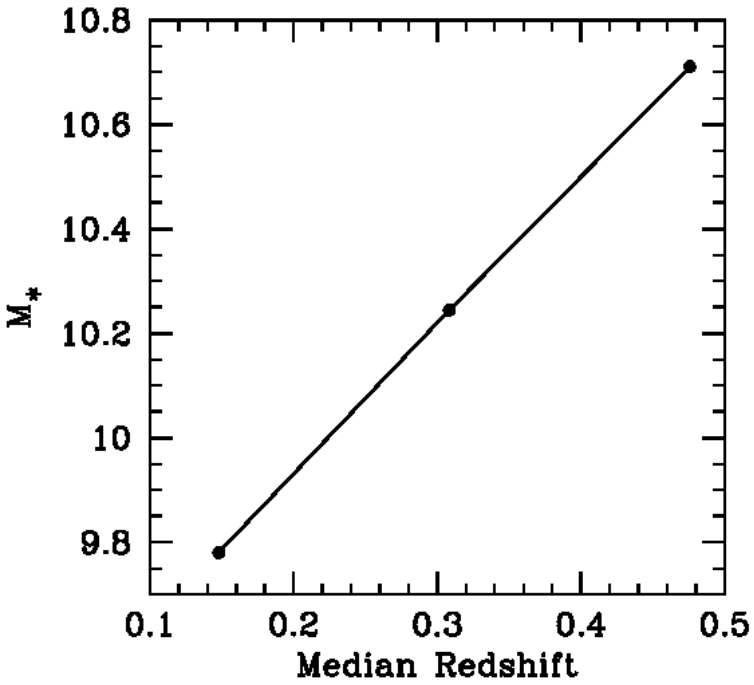

Figure 2.5: The stellar mass completeness limit as a function of redshift for the GEEC sample.

As a summary of the sample sizes involved, Table 2.1 lists the number of GEEC galaxies from the catalogs of Connelly et al. (2012) used in this particular study including the total number, the number of galaxies with available star formation data which is constrained primarily by GALEX coverage (McGee et al., 2011) and the number after completeness cuts. The field sample represents all galaxies that are not confirmed to be in either the optical or X-ray group samples.

Table 2.1: The GEEC galaxy sample.

	Field	X-ray	Optical
Total Number	3800	486	494
Number With Star Formation Data	1705	197	343
Number After Completeness Cuts	599	102	206

2.2 COSMOS

The Cosmological Evolution Survey (COSMOS) (Scoville et al., 2007) covered an area of the sky of approximately 2 deg^2 to a redshift of $\sim$3 (Lilly et al., 2007). There were approximately 200 X-ray (George et al., 2011) and approximately 1500 optically (Knobel et al., 2009, 2012) selected groups identified in the COSMOS field. Spectroscopic data measured by the zCOSMOS team (Lilly et al., 2007) results in approximately 6400 field, 1200 X-ray and 4600 optical group galaxies respectively with spectroscopic redshifts available. The field sample represents those galaxies which have not been confirmed as X-ray or optical group members in the catalogs of George et al. (2011) and Knobel et al. (2012) respectively. The COSMOS survey obtained data from the radio to the X-ray using such instruments as the Hubble Space Telescope, Spitzer, GALEX, XMM-Newton and Chandra with spectroscopic data from the VLT and Magellan (Scoville et al., 2007)[1].

Figure 2.6 shows the distribution of group redshift (left), total group mass (right) and X-ray luminosities (bottom) for the X-ray and optical groups. Only the X-ray groups are shown in the bottom panel. The group masses here for the X-ray groups are estimated from L_x-σ scaling relations generated by Leauthaud et al. (2010) while for optical groups the mass is estimated from the mock catalogs of Kitzbichler & White (2007) which are based on the Millennium simulations of Springel et al. (2005). The redshifts cover a similar distribution while the COSMOS X-ray groups are systematically at the higher mass end. The group masses of the GEEC sample

[1]More information on the COSMOS survey is available at `http://www.astro.caltech.edu/~cosmos`

of Figure 2.1 extend to slightly higher masses than for the COSMOS sample. The bottom panel of Figure 2.6 shows the X-ray luminosities of the X-ray groups cover a range of approximately 41.2<log(L_x) (erg/s)<44, which is a similar range as the X-ray luminosities of the GEEC X-ray group sample from Figure 2.1.

Figure 2.7 shows the redshift (left), stellar mass (right) and Sérsic index (bottom) distributions for field, X-ray and optical group galaxies. The stellar masses were found from deep imaging spanning UV, visible and IR wavelengths (George et al., 2011; Bundy et al., 2006) and from SED fitting (Knobel et al., 2012). The Sérsic indices were found using high resolution imaging from the HST and were found from single Sérsic fits to the two-dimensional surface brightness distributions of the galaxies, as completed by Scarlata et al. (2007) and Sargent et al. (2007) using the Galaxy Image 2D (GIM2D) software (Marleau & Simard, 1998). GIM2D is an IRAF package designed to perform detailed surface brightness fitting. Scarlata et al. (2007) and Sargent et al. (2007) use GIM2D to fit the surface brightness of the galaxies to a single Sérsic profile of the form

$$\Sigma(r) = \Sigma(R_{1/2})\, exp\left\{-k\left[\left(\frac{r}{R_{1/2}}\right)^{1/n} - 1\right]\right\} \tag{2.4}$$

where n is the Sérsic index and k is chosen such that $R_{1/2}$ represents the radius containing half of the total flux. Fitting the galaxy surface brightness to this profile provides estimates for the Sérsic indices of the galaxies. As will be discussed in more detail in Chapter 4, galaxies with a Sérsic index less than 1.5 will be considered disky.

As was done for the GEEC data set, stellar mass incompleteness was accounted for in the COSMOS sample. For simplicity, a conservative single stellar mass completeness cut of $10^{10.6} M_{\odot}$ was applied to the COSMOS group galaxies at all redshifts. This cutoff was found by finding the turnover of the stellar mass distribution at the highest redshift range of the COSMOS data of 0.8-1 (similar to the procedure described in Figure 2.4). Due to the larger sample size of COSMOS this conservative cut still produced a large sample to investigate.

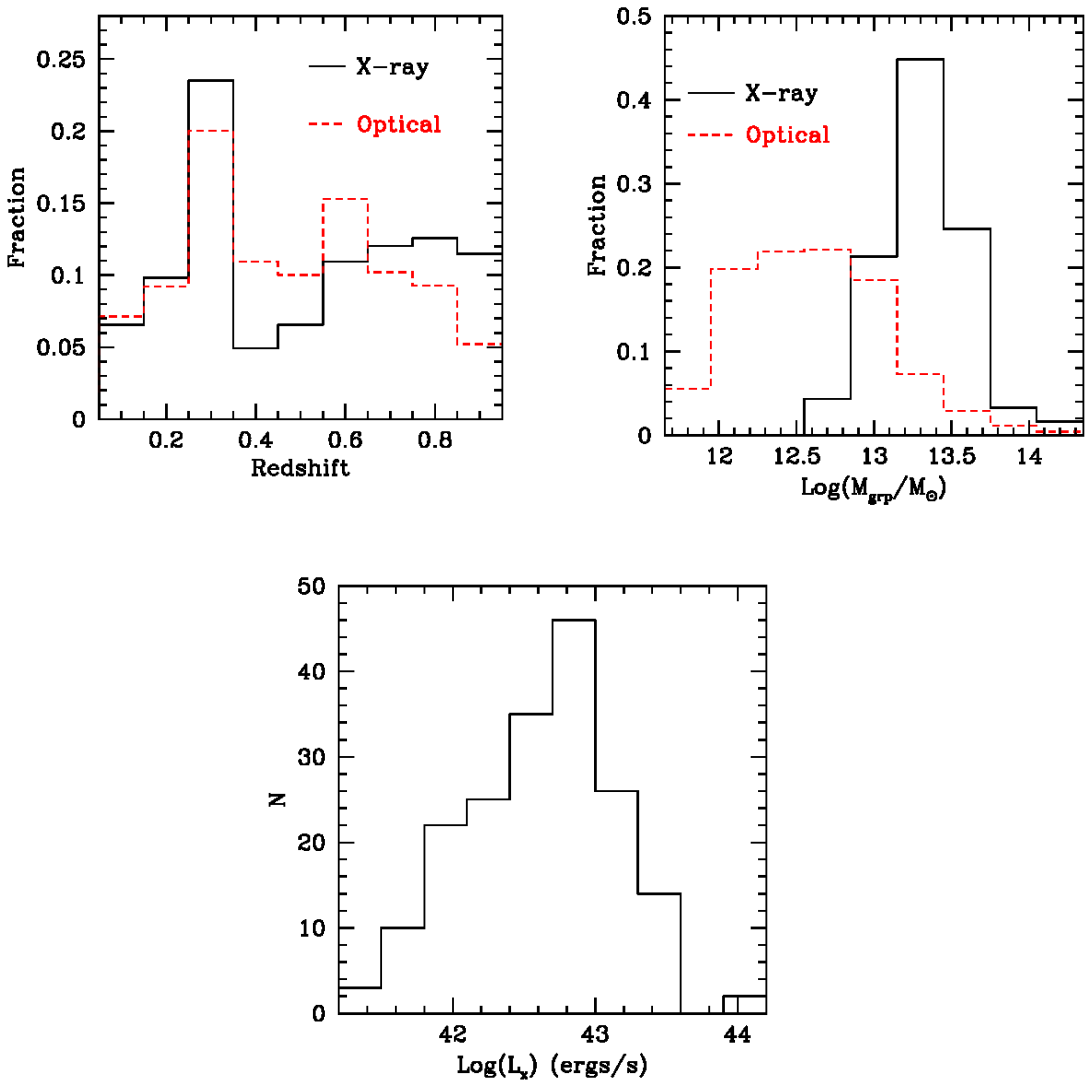

Figure 2.6: Distribution of redshifts (left), total group mass (right) and X-ray luminosities (bottom) for the X-ray and optical COSMOS groups. Only X-ray groups are included in the bottom panel.

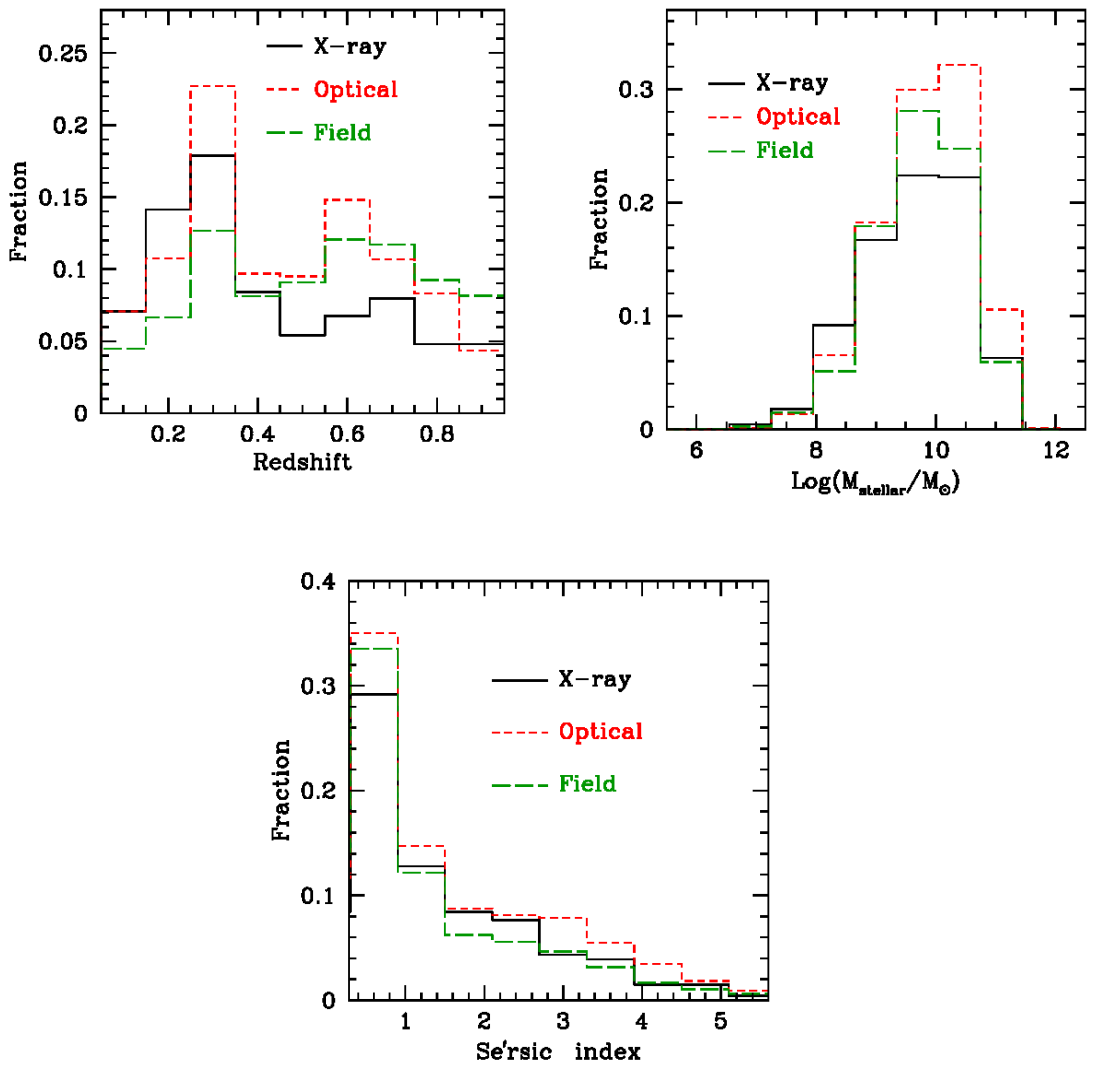

Figure 2.7: Distributions of redshift (left), total stellar mass (right) and Sérsic index (bottom) for COSMOS galaxies in the field and in X-ray and optical groups.

Table 2.2 summarizes the total number of COSMOS galaxies used in this particular study using the X-ray catalogs of George et al. (2011) and the optical catalogs of Knobel et al. (2012). It includes the total number of galaxies with spectroscopic data available, the number of galaxies with Sérsic index measurements available and the number of galaxies after completeness cuts for the field and for the X-ray and optical groups.

Table 2.2: The COSMOS galaxy sample.

	Field	X-ray	Optical
Total Number	6433	1230	4613
Number With Sérsic Indices	6202	665	3846
Number After Completeness Cuts	2025	170	1329

It should be emphasized that unless otherwise stated all of the results that follow for both GEEC passive and COSMOS disk fractions are stellar mass complete using the completeness cuts described above.

Bibliography

Balogh, M. L., McGee, S. L., Wilman, D. J., et al., 2009, MNRAS, 398, 754

Bundy, K., Ellis, R. S., Conselice, C. J., et al., 2006, ApJ, 651, 120

Carlberg, R. G., Yee, H. K. C., Morris, S. L., et al., 2001, ApJ, 552, 427

Connelly, J. L., Wilman, D. J., Finoguenov, A., et al., 2012, ApJ, 756, 139

Finoguenov, A., Connelly, J. L., Parker, L. C., et al., 2009, ApJ, 704, 564

George, M. R., Leauthaud, A., Bundy, K., et al., 2011, ApJ, 742, 125

Hogg, D. W., 1999, arXiv:9905116

Kitzbichler, M. G. & White, S. D. M., 2007, MNRAS, 376, 2

Knobel, C., Lilly, S. J., Iovino, A., et al., 2009, ApJ, 697, 1842

Knobel, C., Lilly, S. J., Iovino, A., et al., 2012, ApJ, 753, 121

Leauthaud, A., Finoguenov, A., Kneib, J-P., et al., 2010, ApJ, 709, 97

Lilly, S. J., Le Fèvre, O., Renzini, A., et al., 2007, ApJS, 172, 70

Marleau, F. R. & Simard, L., 1998, ApJ, 507, 585

McGee, S. L., Balogh, M. L., Wilman, D. J., et al., 2011, MNRAS, 413, 996

Sargent, M. T., Carollo, C. M., Lilly, S., et al., 2007, ApJS, 172, 434

Scarlata, C., Carollo, C. M., Lilly, S., et al., 2007, ApJS, 172, 406

Scoville, N., Aussel, H., Brusa, M., et al., 2007, ApJS, 172, 1

Springel, V., White, S. D. M., Jenkins, A., et al., 2005, Nature, 435, 629

Wilman, D. J., Balogh, M. L., Bower, R. G., et al., 2005, MNRAS, 358, 71

Yee, H. K. C., Morris, S. L., Lin, H., et al., 2000, ApJS, 129, 475

Chapter 3

Passive Fractions

One of the basic observational properties of galaxies is their star formation rate. In order to ascertain the effect of host environment on galaxy evolution we measure the fraction of non-star-forming galaxies, called the passive or quiescent fraction, f_q, as a function of environment. The passive fraction is defined as

$$Passive\,Fraction = \frac{\#\,of\,galaxies\,with\,sSFR < 10^{-11}yr^{-1}}{total\,\#\,of\,galaxies} \tag{3.1}$$

where sSFR was given in Equation 2.3 where, as was discussed in Section 2.1, galaxies with sSFR $> 10^{-11}yr^{-1}$ are considered star-forming while those with sSFR $< 10^{-11}yr^{-1}$ are considered non-star-forming or passive. Using the GEEC sample, these passive fractions were computed as a function of a number of parameters such as overall environment, group mass, group-centric distance, X-ray luminosity and redshift and will be presented in the following sections.

3.1 Environment

It is well known that there is a strong SFR-stellar mass relationship for galaxies where higher mass galaxies typically have less star formation (e.g. McGee et al., 2011; Whitaker et al., 2012). Figure 3.1 shows the passive fraction as a function of

stellar mass for field, X-ray and optical group galaxies. Galaxies were separated into stellar mass bins with the location of the points representing the median stellar mass in each bin. The error bars are calculated following the methodology of Cameron (2011) for calculating errors on fractions. The lines represent weighted linear least squares fits. The slopes of the best fit lines are 0.3 ± 0.1, 0.2 ± 0.2 and 0.2 ± 0.1 for the field, X-ray and optical group galaxies respectively. The errors on the slopes were found by finding the maximum and minimum slopes that fit the data.

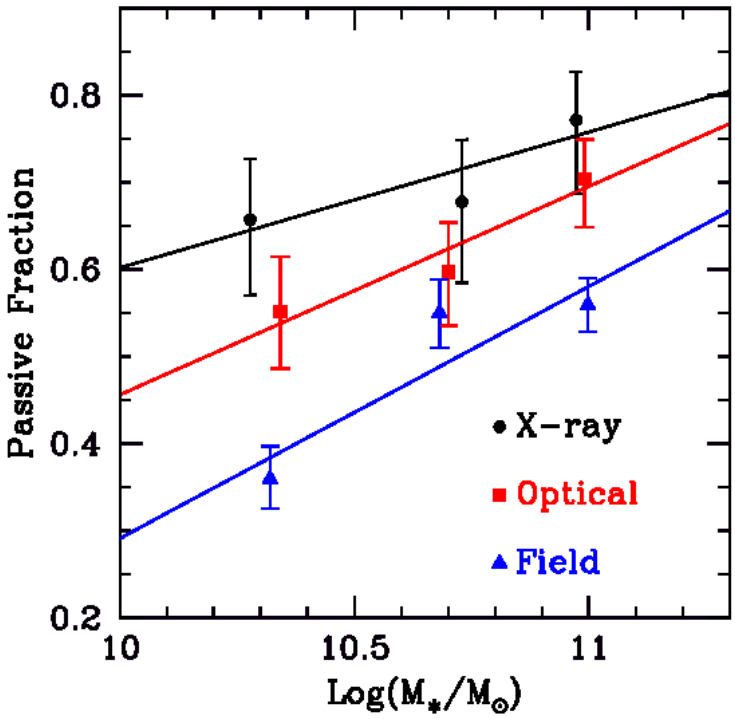

Figure 3.1: Passive fraction as a function of stellar mass for field, X-ray and optical group galaxies. The passive fraction is higher for group galaxies than the field galaxies and is higher for the X-ray group galaxies compared to the optical group galaxies. The slopes of the best fit lines are 0.3 ± 0.1, 0.2 ± 0.2 and 0.2 ± 0.1 for the field, X-ray and optical group galaxies respectively.

The passive fraction clearly increases with stellar mass (a trend which has been previously observed (McGee et al., 2011) and will be consistently observed throughout

this thesis) with the group galaxies having a higher passive fraction than that of the field. This agrees with the results of Giodini et al. (2012) presented in Figure 1.5 which showed a higher amount of star formation in the field. It is very interesting to note however that for the groups themselves, the X-ray groups have a higher passive fraction than the optical groups suggesting galaxy evolution is different between the two types of groups. The evolutionary processes ongoing in X-ray bright galaxy groups appears to quench star formation when compared with galaxies from optical groups at the same stellar mass. Overall, Figure 3.1 shows that for a galaxy of some given mass, it would likely have more star formation if located in the field than if it was in a group and is most likely to be passive if located in an X-ray group.

An alternative approach to calculating the passive fraction is to look at the median sSFR. Figure 3.2 shows the median sSFR as a function of stellar mass for field, X-ray and optical group galaxies. Similar trends to those in Figure 3.1 are observed, with median sSFR values lower for group galaxies than field galaxies and lowest for the X-ray group galaxies thus showing lower overall star formation in X-ray groups. Both figures also show a wider range in their passive fractions and median sSFR's at lower stellar masses. Moving to higher stellar masses produces less difference suggesting environment plays less of a role for these galaxies. This is consistent with the results of McGee et al. (2011) who also find a larger difference between the passive fractions of field and group galaxies at lower masses and the result also agrees with Peng et al. (2010) and Figure 1.4. The passive fractions and median sSFR's show similar trends but given that estimating the SFR of galaxies with very low sSFR is difficult (McGee et al., 2011) we elect to use passive fractions for the remainder of the star formation analysis. It should be noted that this figure and all figures to follow are for all galaxies detected in X-ray groups and all galaxies detected in optical groups. Excluding galaxies which were found in both X-ray and optically detected groups produced virtually the same result as there was very small overlap in galaxies found in both types of groups, especially after including only those with stellar mass and

SFR measurements and after completeness cuts.

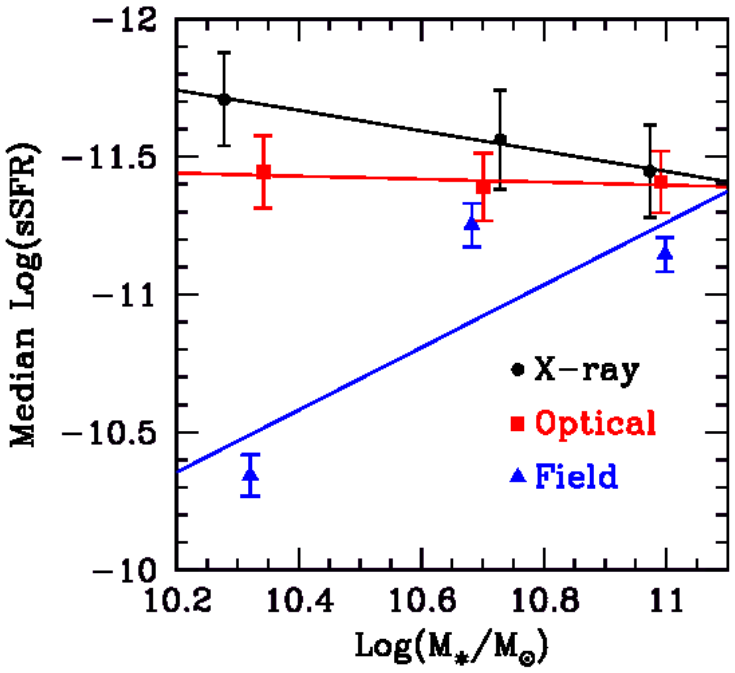

Figure 3.2: Median log(sSFR) as a function of stellar mass for field, X-ray and optical group galaxies. The median value is lower for group galaxies (note the negative signs indicate the median value is lower) than field galaxies and is lower for the X-ray group galaxies than the optical group galaxies. This agrees with the results of Figure 3.1 as both figures show that galaxies in X-ray groups have the lowest amount of star formation.

3.2 Halo Mass

To check for any dependence in the passive fraction on group halo mass Figure 3.3 shows the passive fraction as a function of group mass for both the X-ray and optical groups. At any particular group mass it again shows an overall higher passive fraction for galaxies in X-ray groups. The slopes of the best fit lines are -0.07 $\pm$ 0.07 and 0.01 $\pm$ 0.07 for the X-ray and optical group galaxies respectively. The linear least squares fit

to both groups gives no statistically significant slope. A more thorough analysis of the slope values and these results is left for Chapter 5 where the possible dependencies of passive and disk fractions on halo mass are discussed. Note that galaxies of all stellar masses above the completeness cuts are included in Figure 3.3, and given the strong trend with stellar mass observed in Figure 3.1, in order to investigate environmental trends it is critical to make sure that galaxies with the same stellar mass are being compared.

So, as a further check into the halo mass, Figure 3.4 plots the passive fraction as a function of stellar mass by dividing the sample into galaxies found in low and high mass X-ray and optical groups, with the division determined by the approximate median group mass. Overall, with the exception of low mass galaxies in high mass X-ray groups, there is overlap with all points and neither the low mass or high mass groups show a systematically lower or higher passive fraction, indicating no clear dependence on group mass, in agreement with the results of Hou et al. (2013) shown in Figure 1.7. Thus, for galaxies of a given stellar mass, there will be roughly the same passive fractions irrespective of the halo mass of the group in which they reside. If there is a trend in passive fraction with halo mass it is too small to be detected with our current sample size.

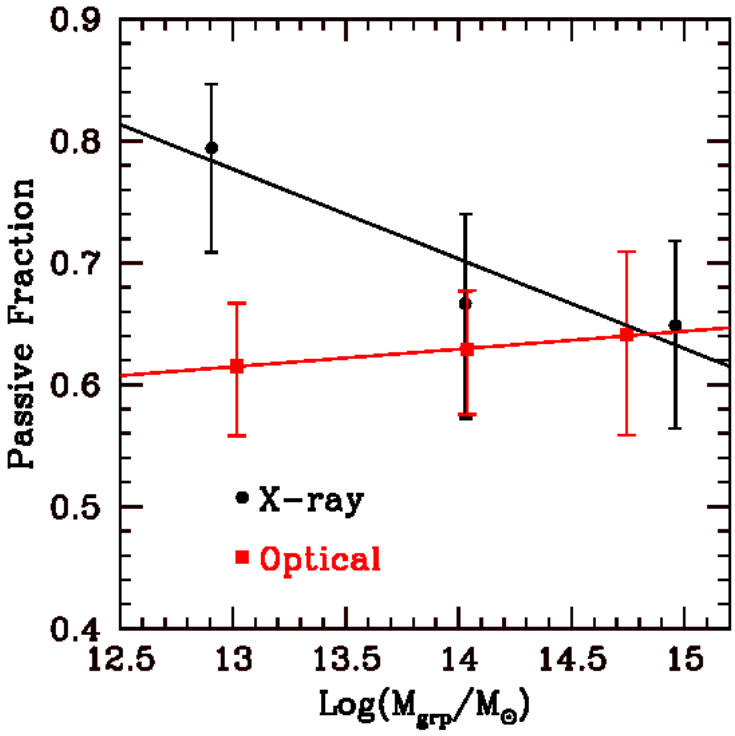

Figure 3.3: Passive fraction as a function of halo mass for galaxies in X-ray and optical groups. Note that galaxies of all stellar masses above the completeness cuts are included in this figure, and given the strong trend with stellar mass observed in Figure 3.1, in order to investigate environmental trends it is critical to make sure that galaxies with the same stellar mass are being compared. The slopes of the best fit lines are -0.07 $\pm$ 0.07 and 0.01 $\pm$ 0.07 for the X-ray and optical group galaxies respectively and thus no trend of passive fraction with group mass is detected within errors for either sample.

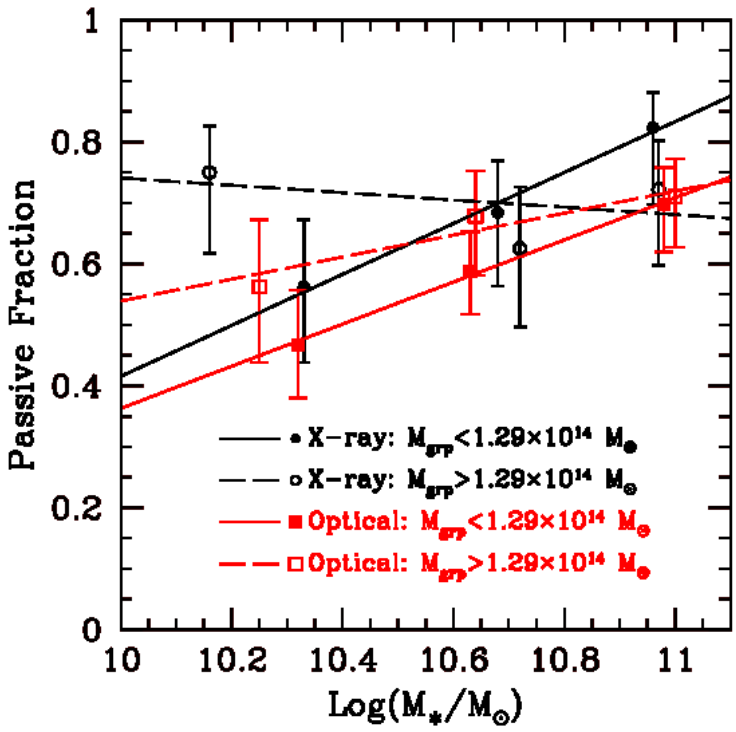

Figure 3.4: Passive fraction as a function of stellar mass for X-ray and optical group galaxies subdivided into low and high mass groups. Most points overlap and thus no strong dependence on total group mass observed.

3.3 Radial Dependencies

In Section 3.2 it was shown that there is no strong dependence of the passive fraction on group mass, but another important parameter to consider which may affect the properties of a galaxy is its location within the group (i.e. its distance from the group centre or its group-centric distance). Figure 3.5 shows the passive fraction as a function of group-centric distance (normalized by r_{200} as defined in Equation 2.2) for X-ray and optical groups. The slopes of the best fit lines are -0.1 $\pm$ 0.2 and -0.1 $\pm$ 0.3 for the X-ray and optical group galaxies respectively. The X-ray group galaxies once again produce a systematically higher passive fraction than the optical group galaxies and both the X-ray and optical group galaxies produce a slope of zero within error. The location of the points represent the median r/r_{200} values from each bin when dividing the X-ray and optical group galaxies into three equal bins. The median values were slightly different in each of the bins for the galaxies of the X-ray and optical groups and explains the offset in the points, especially evident in the second point.

Figure 3.6 acts to further investigate any possible radial trends by plotting the passive fraction for galaxies in the inner and outer parts of X-ray and optical groups defined as galaxies within $0.5r_{200}$ and outside of $0.5r_{200}$ respectively. Similarly to the group mass results of Figure 3.4, most of the points overlap showing no clear difference. For galaxies at a given stellar mass, there is no clear difference in passive fractions between those in the inner and outer parts of the groups. The point representing low mass galaxies in the central regions of the X-ray groups is an outlier. Comparing this point with the outlier point in Figure 3.3 for low mass galaxies in high mass groups, passive fractions appear to be boosted for low mass galaxies that are found in the inner regions of the groups and located in high mass groups. This is an interesting trend which should be followed up with larger data sets.

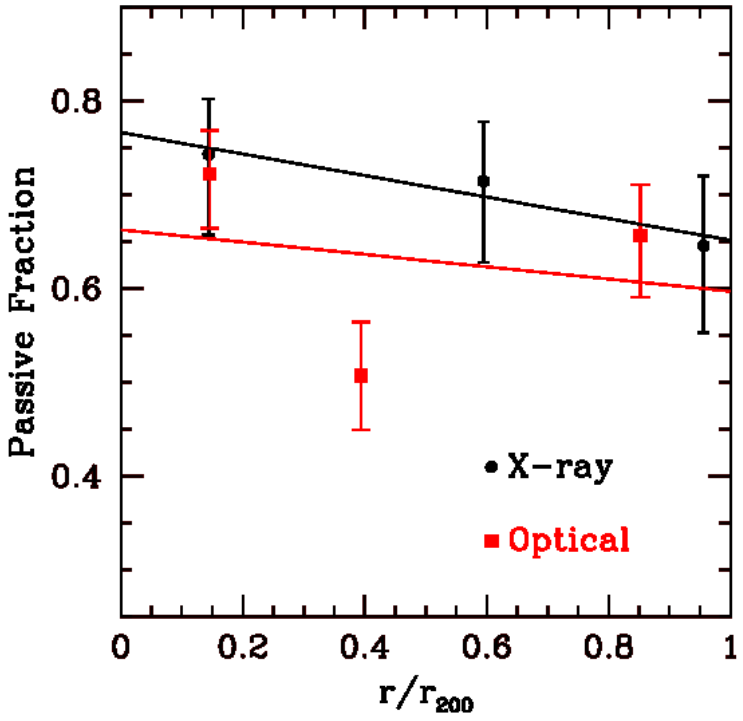

Figure 3.5: Passive fraction as a function of group-centric distance for X-ray and optical group galaxies. The slopes of the best fit lines are -0.1 ± 0.2 and -0.1 ± 0.3 for the X-ray and optical group galaxies respectively and thus no trend of passive fraction with radius is detected within errors for either sample.

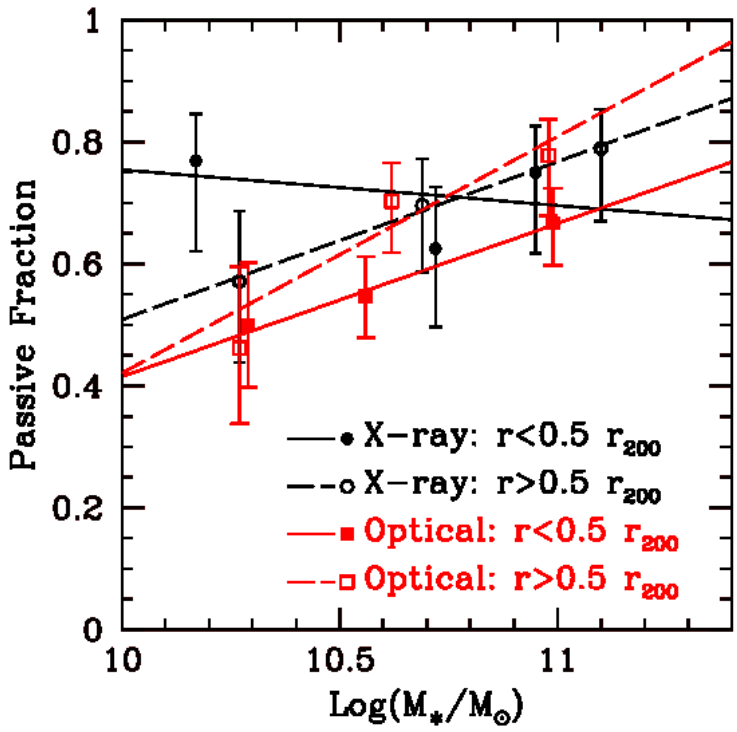

Figure 3.6: Passive fraction as a function of stellar mass for X-ray and optical group galaxies in two group-centric bins. Most points overlap and thus no strong dependence on distance from the group center is observed.

3.4 X-ray Luminosity

It has been shown above in Figure 3.1 that differences exist between the passive fractions within the X-ray bright and faint groups. This section searches for correlations with X-ray luminosity for the X-ray groups. Figure 3.7 shows the passive fraction as a function of X-ray luminosity. No strong relation is observed with a calculated slope consistent with zero. This is interesting based on the differences between the X-ray and optical groups shown in Figure 3.1. Since the X-ray groups were found to have a higher passive fraction one may have expected the groups with higher X-ray luminosities to show higher passive fractions

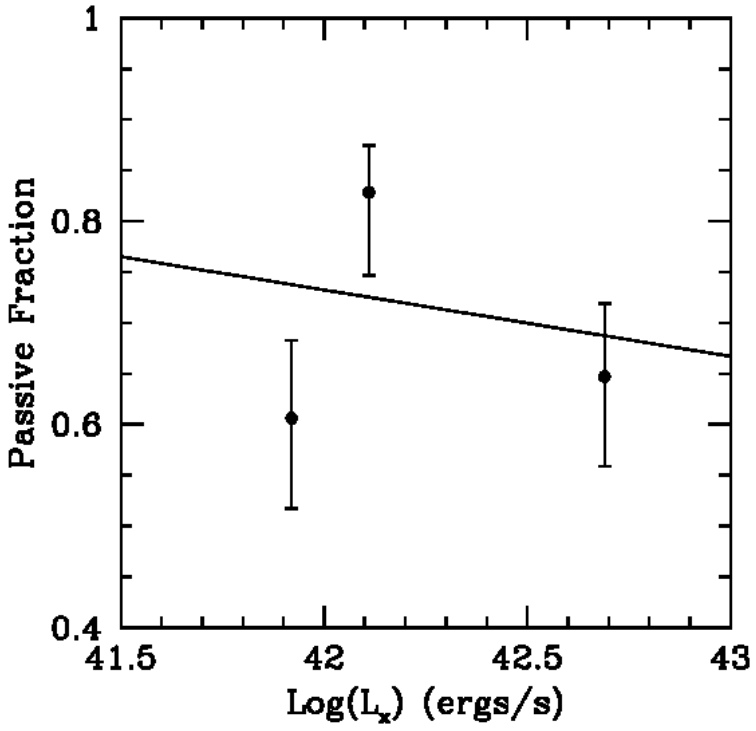

Figure 3.7: Passive fraction as a function of X-ray luminosity. No obvious dependence on X-ray luminosity is observed.

3.5 Redshift

Previous work has shown that the amount of star formation increases with redshift (as was shown in Figure 1.5 taken from Giodini et al., 2012). Figure 3.8 explores the passive fractions as a function of redshift for the GEEC sample. The left panel is for the stellar mass complete sample using the cuts as summarized in Figure 2.5. For each of the field, X-ray and optical group galaxies, no redshift dependence is observed. However, because of the completeness cuts applied as described in Section 2.1, different redshift bins will have different stellar mass distributions. The lowest redshift bin will have contributions from a wide range of galaxy masses while the highest redshift bin will only include high mass galaxies and thus a fair comparison in the passive fractions at each redshift cannot be made from this particular figure.

To attempt to correct for this, the right hand panel of Figure 3.8 plots the passive fraction as a function of redshift using a conservative single stellar mass cut of $10^{10.7} M_{\odot}$ (the turnover value from the highest redshift interval used to determine completeness limits). Signs of decreasing passive fraction with redshift are observed, especially evident for the field, however the trend is still not obvious in the X-ray or optical groups.

To further investigate a redshift trend for the GEEC sample, Figure 3.9 plots the passive fraction as a function of redshift but only for field and group galaxies in the narrow stellar mass range $10.8<\log(M_*/M_{\odot})<11$ (note that similar results are obtained for any narrow range in stellar mass). This was done to eliminate any discrepancies that may have been caused by differences in stellar mass which has been shown to cause a strong effect on passive fraction. Making this cut significantly reduces the X-ray and optical group galaxy sample sizes. Thus for Figure 3.9 both group samples were combined to increase statistics and thus are labeled as the total group sample. In this case, the redshift trend is evident and the passive fraction decreases with redshift confirming more star formation at higher redshift in both the group and field populations.

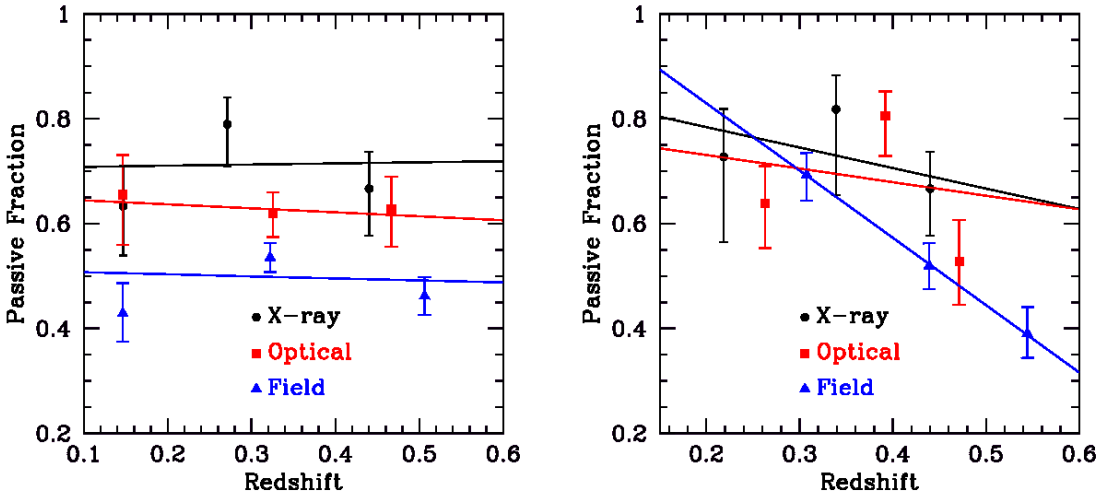

Figure 3.8: Passive fraction as a function of redshift for field, X-ray and optical group galaxies. The left panel is for the stellar mass complete sample with different completeness limits at each redshift while the right panel is for a single stellar mass cut of $10^{10.7} M_{\odot}$. There is no detectable trend within error in passive fraction with redshift observed in the left panel while the right panel does show signs of a decreasing passive fraction, especially in the field, but there is no detectable trend within error in passive fraction with redshift for the X-ray or optical group galaxies.

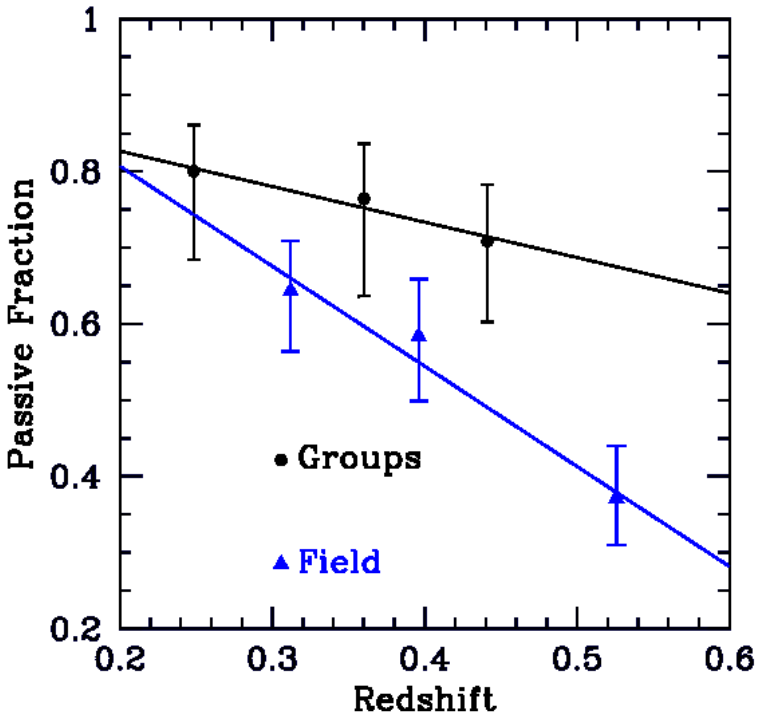

Figure 3.9: Passive fraction as a function of redshift for field and groups for the stellar mass range $10.8<\log(M_*/M_\odot)<11$. Note here that the group sample combines the X-ray and optical group galaxies in order to have a sufficient sample size. The passive fraction decreases with increasing redshift.

3.6 Total Group Stellar Mass

In addition to the group halo mass, total group stellar masses have been determined for the GEEC sample as in Connelly et al. (2012). It should be noted that since low mass galaxies generally go undetected, especially at higher redshift, corrections have been made so that the stellar mass estimates take into account these low mass galaxies and thus give an accurate group stellar mass estimate.

Figure 3.10 shows the passive fraction subdivided by groups of low and high total stellar mass. There is some scatter for the first two bins but similarly to the halo mass, there is no strong trend with group stellar mass. For a galaxy of given stellar mass, there is no obvious trend with the total stellar mass of the parent groups.

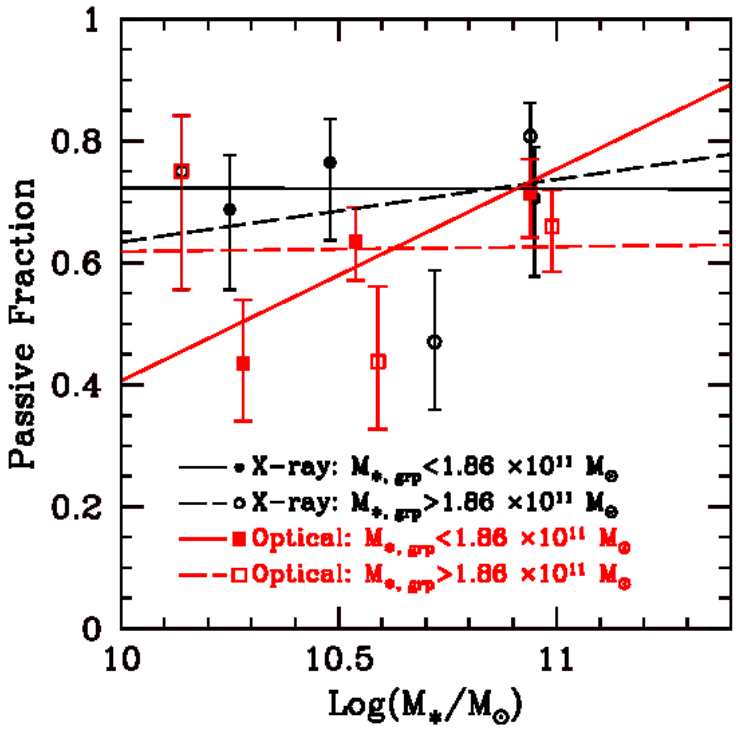

Figure 3.10: Passive fraction as a function of stellar mass for X-ray and optical group galaxies in two total group stellar mass bins. There is no strong dependence on the total group stellar mass.

3.7 Mass Segregation

An active question in the study of galaxy groups is whether or not mass segregation occurs (Ziparo et al., 2013), i.e. whether or not high mass galaxies settle near the centres of group halos. Mass segregation is important as it can be used as a tracer of the current evolutionary state of a system. For example, relaxed, evolved systems may have a massive galaxy at the centre of their potential wells which may produce a mass gradient as a function of radius while less evolved systems may lack a massive galaxy at their centres and therefore may not show signs of mass segregation. Figure 3.11 shows the mean log stellar mass as a function of group-centric distance. The left panel is for all galaxies above the redshift dependent stellar mass completeness

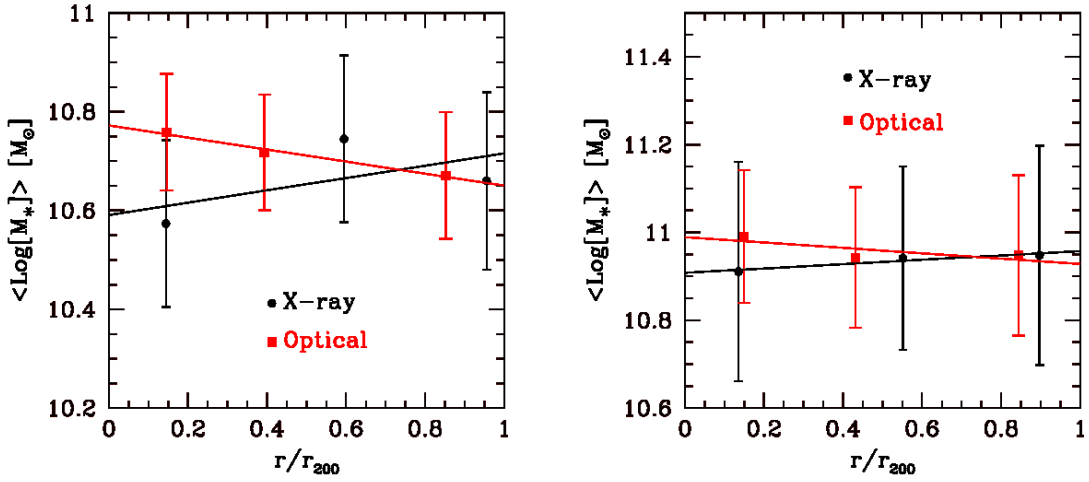

Figure 3.11: Average galaxy stellar mass as a function of group-centric distance. The left panel uses the stellar mass cuts as a function of redshift (from Figure 2.5) while the right panel is for a single stellar mass cut of $10^{10.7} M_{\odot}$.

limits for GEEC while the right panel shows the results using a single mass cutoff of $10^{10.7} M_{\odot}$.

For both panels the X-ray and optical group galaxies produced slopes consistent with zero. Mass segregation in groups is still a matter of debate and will be further investigated for the COSMOS sample in Section 4.6.

Bibliography

Cameron, E., 2011, PASA, 28, 128

Connelly, J. L., Wilman, D. J., Finoguenov, A., et al., 2012, ApJ, 756, 139

Giodini, S., Finoguenov, A., Pierini, D., et al., 2012, A&A, 538, A104

Hou, A., Parker, L. C., Balogh, M. L., et al., 2013, MNRAS, 435, 1715

McGee, S. L., Balogh, M. L., Wilman, D. J., et al., 2011, MNRAS, 413, 996

Peng, Y.-j., Lilly, S. J., Kovač, K., et al., 2010, ApJ, 721, 193

Whitaker, K. E., van Dokkum, P. G., Brammer, G., et al., 2012, ApJL, 754, L29

Ziparo, F., Popesso, P., Biviano, A., et al., 2013, MNRAS, 434, 3089

Chapter 4

Disk Fractions

Another useful way to characterize environmental effects on galaxy evolution is by looking at galaxy morphologies by calculating the fraction of galaxies with prominent disks. Whether a galaxy is currently designated as a spiral, elliptical or S0 for example and whether or not it will go through significant morphological changes is strongly dependent on its environment. The morphology of a galaxy can be inferred by eye but quantitative galaxy surface brightness fitting programs such as Galaxy Image 2D (GIM2D) (Marleau & Simard, 1998) are also used to fit two component models with a bulge and a disk to large samples of galaxies, where it is impractical to visually classify each galaxy.

Disk galaxies typically have a Sérsic index around 1 while elliptical galaxies typically have a Sérsic index near 4. For this thesis, galaxies with a Sérsic index less than 1.5 were considered disky while those with a Sérsic index greater than 1.5 were not considered disky. This cut was chosen by looking at the Sérsic index distributions in the bottom panel of Figure 2.7. The peak occurs at a Sérsic index of approximately 1 representing the disk-like galaxies. Thus, a cut of 1.5 was sufficient in dividing the disk-like galaxies from the non-disk-like galaxies (Note however that the results were insensitive to this exact choice of value for the Sérsic index used to define the disky galaxies, as described in detail in the following section). So, the disk fraction, f_D, is

given by

$$Disk\,Fraction = \frac{\#\,of\,galaxies\,with\,Sérsic\,index < 1.5}{total\,\#\,of\,galaxies} \tag{4.1}$$

The disk fractions were calculated for the COSMOS sample with the Sérsic indices obtained from single Sérsic fits taken from the measurements of Scarlata et al. (2007) and Sargent et al. (2007) using GIM2D (Marleau & Simard, 1998) as described in Section 2.2. The disk fractions were calculated as a function of overall environment, group halo mass, group-centric distance, X-ray luminosity and redshift and the results will be presented in the subsequent sections. For the case of COSMOS, galaxies that were classified in both the X-ray and optical group samples were excluded so that the X-ray group galaxies were only in the X-ray sample and the optical group galaxies were only in the optical sample, i.e. there was no overlap between the group galaxies used for the analysis of this chapter.

4.1 Environment

It is now well known that morphology-density relations exist with higher elliptical fractions typically observed in denser regions such as in the centres of rich clusters (Dressler, 1980; Butcher & Oemler, 1978). Figure 4.1 shows the disk fraction for the COSMOS survey as a function of galaxy stellar mass for field, X-ray (George et al., 2011) and optical (Knobel et al., 2012) group galaxies. The slopes of the best fit lines are -0.66 $\pm$ 0.08, -0.3 $\pm$ 0.1 and -0.29 $\pm$ 0.07 for the field, X-ray and optical group galaxies respectively. The disk fraction clearly decreases with increasing stellar mass (a trend consistently observed throughout this chapter) suggesting a larger fraction of massive galaxies are early-types. Figure 4.1 shows that there are typically more disky galaxies in the field compared to groups. Also observable is that the disk fraction appears higher for galaxies in X-ray groups than galaxies in optical groups again suggesting evolution is different between the two types of groups as was seen for the

passive fractions of Figure 3.1. The group mass distribution in the right panel of Figure 2.6 shows that the X-ray groups are skewed at the high mass end. However, Section 4.2 below will show that the disk fraction does not depend strongly on group mass and hence the differences in disk fractions observed in Figure 4.1 are not a result of the disparity in the halo masses between the X-ray and optical groups.

The higher disk fraction calculated for galaxies in X-ray groups is interesting based on the previous results of Figure 3.1 where the passive fraction was also higher for X-ray group galaxies compared to the optical group galaxies. Since star-forming galaxies are typically found to be disky (since they typically have higher amounts of gas in which to form stars) (Poggianti et al., 2009) a higher passive fraction would perhaps be predicted to correlate with a lower disky fraction, but the opposite trend is observed. It is also known that at higher redshifts a higher fraction of spirals is observed (Dressler et al., 1997). Thus perhaps the X-ray group galaxies contributing to the results of Figure 4.1 are skewed to higher redshifts. To check this, a two sample Kolmogorov-Smirnov test was applied to the redshift distributions of the X-ray and optical group galaxies concluding that both distributions are actually drawn from the same distribution at a 95% confidence level. Therefore, the difference cannot be simply attributed to any differences in redshifts. This suggests galaxy morphology and star formation may not be showing the same trends in X-ray and optical groups. However, the passive and disk fractions come from two separate samples and so a direct comparison is difficult to make. This will be discussed further in Chapter 5.

As mentioned above, the choice of a Sérsic cutoff of 1.5 as the division between disky and non-disky galaxies was arbitrary but the results were insensitive to this choice of value. Figure 4.2 again shows the disk fraction but assuming galaxies with a Sérsic index less than 2 are disky. Similar trends are obtained as found in Figure 4.1 which used a Sérsic cutoff of 1.5.

As another check of the morphology relation, the median Sérsic index is plotted in Figure 4.3 as a function of stellar mass. Again, similar conclusions can be drawn

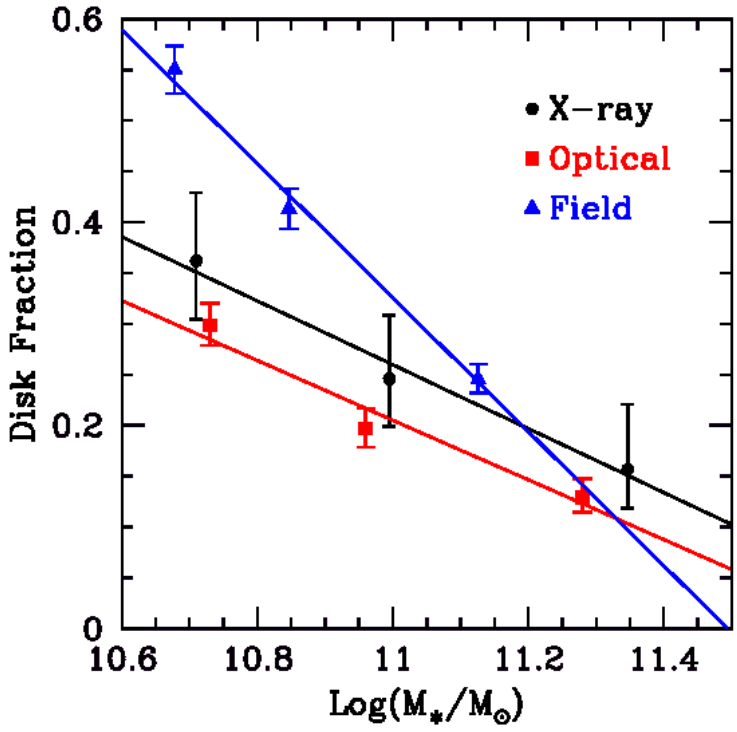

Figure 4.1: Disk fraction as a function of stellar mass for field, X-ray and optical group galaxies. The disk fraction is higher for the field than for group galaxies and is higher for the X-ray groups than the optical groups. The slopes of the best fit lines are -0.66 ± 0.08, -0.3 ± 0.1 and -0.29 ± 0.07 for the field, X-ray and optical group galaxies respectively.

as in the results of Figure 4.1. As a reminder, disky galaxies typically have a Sérsic index of approximately 1 while the Sérsic index for more bulge-dominated galaxies is typically around 4. So, the lower median values for the field suggest more disk-like galaxies in the field in comparison to groups and again more disk-like galaxies in X-ray groups in comparison to optical groups.

It also interesting to note that the disk fractions of figures 4.1 and 4.2 and the median Sérsic indices of 4.3 all show less difference at higher mass perhaps indicating that the fraction of disk galaxies approaches a constant for higher mass galaxies and environment may play less a role, consistent with Figure 1.4 as discussed in Peng et

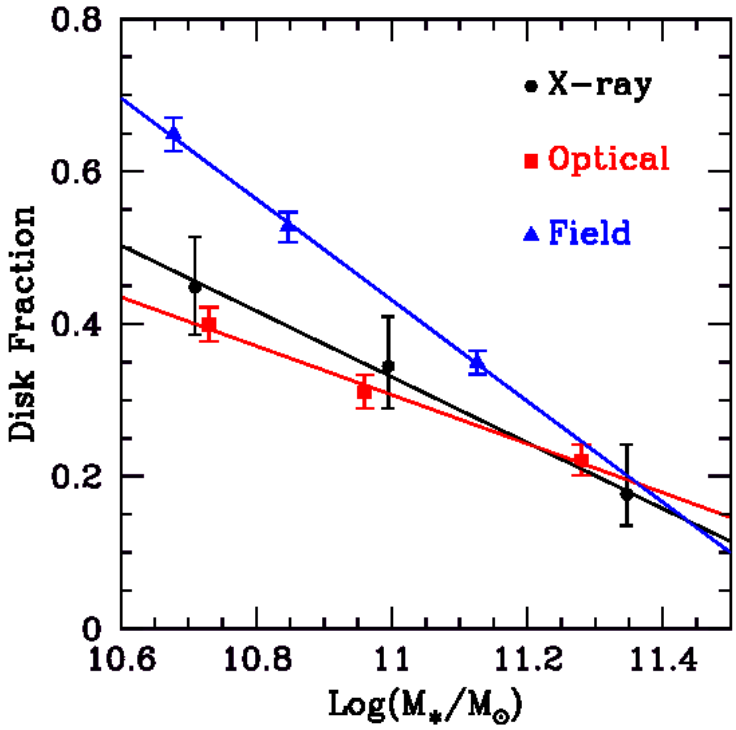

Figure 4.2: Disk fraction as a function of stellar mass for field, X-ray and optical group galaxies but using a Sérsic cutoff of 2 to define disky galaxies. Similar results are obtained as found in Figure 4.1 which used a Sérsic cutoff of 1.5. Thus, the overall disk fraction trends are insensitive to the exact value for the Sérsic index used to define disky galaxies. The disk fraction is higher for the field than for group galaxies and is higher for the X-ray group galaxies than the optical group galaxies.

al. (2010). A similar effect was seen for the passive fractions as discussed in Section 3.1 with higher mass galaxies showing less difference in their passive fractions as a function of environment. For the remainder of this thesis, disk fractions were defined using a Sérsic index cut of 1.5.

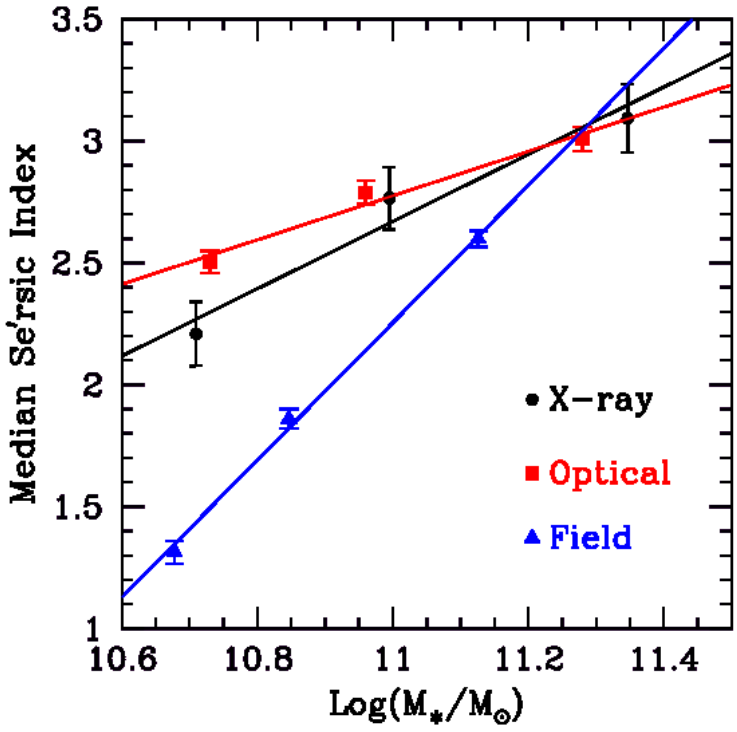

Figure 4.3: Median Sérsic index as a function of stellar mass for field, X-ray and optical group galaxies. The results are similar to those found in Figure 4.1. The Sérsic index is lower for the field than for group galaxies and is lower for the X-ray group galaxies than the optical group galaxies.

4.2 Halo Mass

To check for any dependence of the disk fraction on group mass Figure 4.4 plots the disk fraction as a function of total group mass for the X-ray and optical groups. The slopes of the best fit lines are -0.1 $\pm$ 0.2 and -0.02 $\pm$ 0.03 for the X-ray and optical group galaxies respectively. X-ray groups once again show a higher overall disk fraction but there is no clear dependence on group mass as confirmed from the linear least squares fits which produced slopes consistent with zero within errors.

To further check for any dependence in the disk fraction on group mass Figure 4.5 plots the disk fraction for low mass and high mass X-ray and optical groups with the division representing the median group mass. Overall, there is very strong

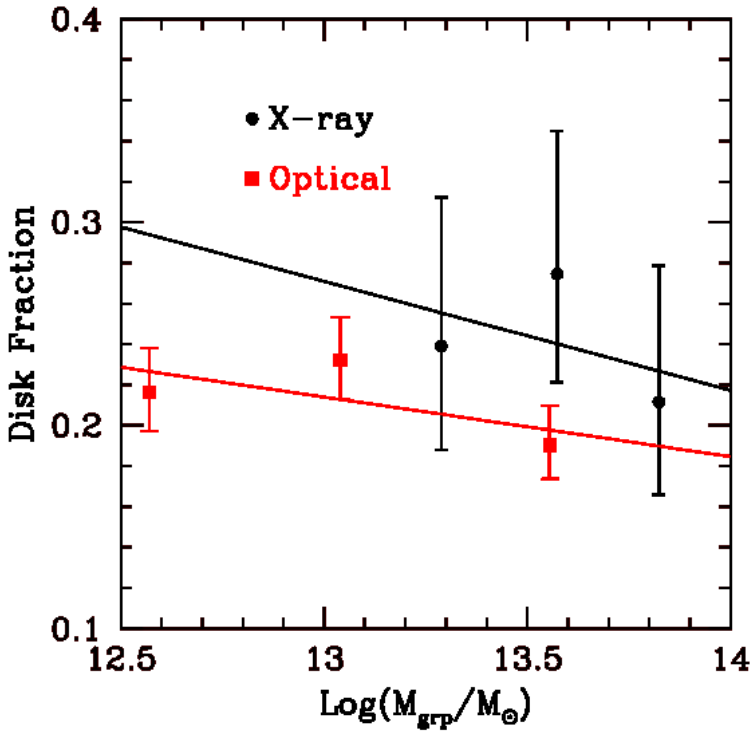

Figure 4.4: Disk fraction as a function of group halo mass for X-ray and optical group galaxies. There is no strong dependence on group mass. The slopes of the best fit lines are -0.1 ± 0.2 and -0.02 ± 0.03 for the X-ray and optical group galaxies respectively.

overlap between the low and high mass groups showing no clear dependence on group mass. Thus for a galaxy of given stellar mass, its morphology does not appear to be determined by its group halo mass.

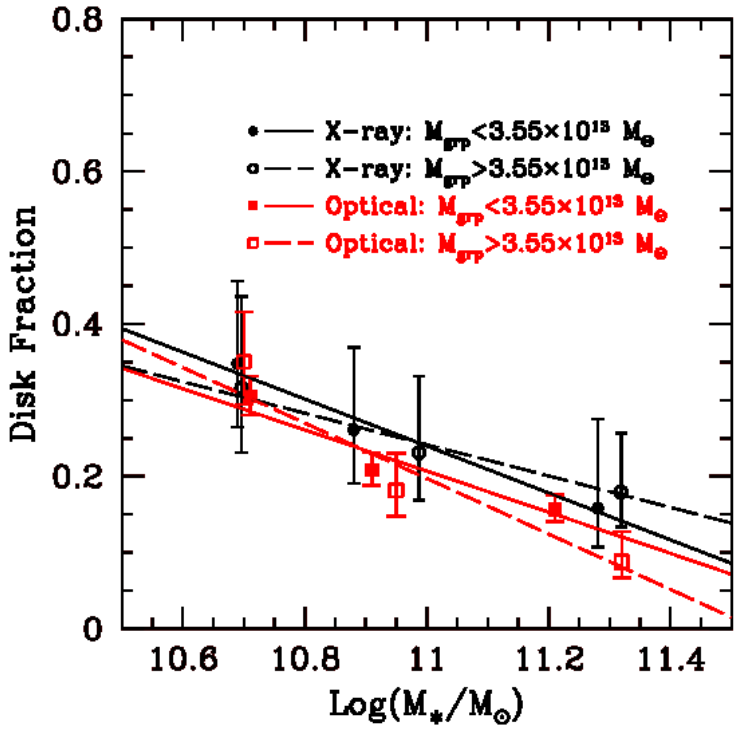

Figure 4.5: Disk fraction as a function of stellar mass for X-ray and optical group galaxies subdivided into low and high mass groups. There is no strong dependence on group mass as the points for galaxies in low mass and high mass groups overlap.

4.3 Radial Dependencies

This section investigates whether or not the location in which galaxies are located within a group will affect the disk fractions. Figure 4.6 plots the disk fraction as a function of group-centric distance (normalized by r_{200}) for X-ray and optical groups. The slopes of the best fit lines are 0.2 $\pm$ 0.2 and 0.08 $\pm$ 0.07 for the X-ray and optical group galaxies respectively. In this case, the X-ray group results show no significant slope while the optical groups slope is statistically significant (1-σ) and positive suggesting that the fraction of disky galaxies is higher in the outer parts of groups, consistent with Butcher & Oemler (1978).

It has been shown in Figure 4.1 for example that stellar mass must be considered

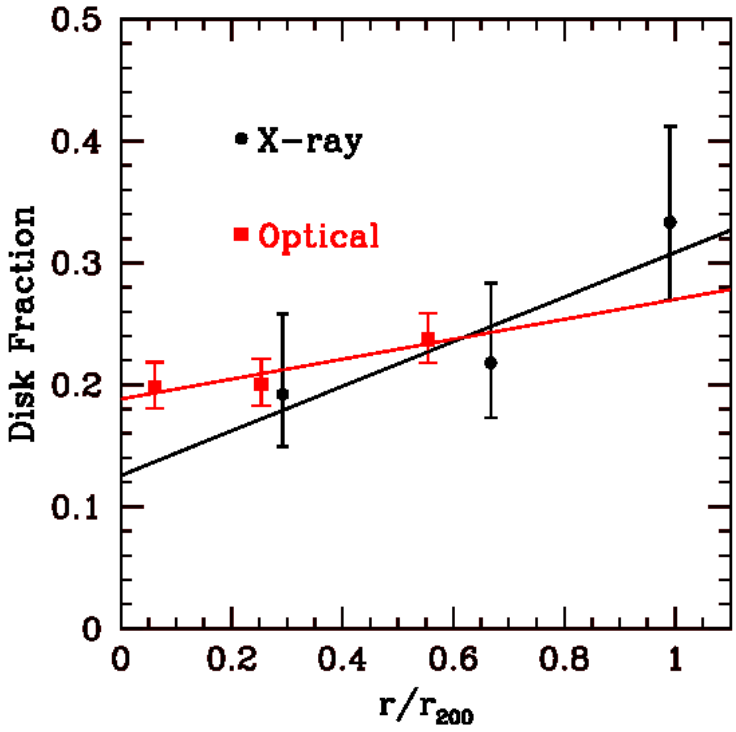

Figure 4.6: Disk fraction as a function of group-centric distance for X-ray and optical group galaxies. The fraction of disky galaxies appears to increase in moving away from the group centre. The slopes of the best fit lines are 0.2 ± 0.2 and 0.08 ± 0.07 for the X-ray and optical group galaxies respectively.

when studying galaxy properties. So, as a further check into possible radial trends, Figure 4.7 plots the disk fraction as a function of galaxy stellar mass for galaxies inside and outside $0.5r_{200}$. The points for galaxies inside and outside $0.5r_{200}$ mostly overlap at each stellar mass suggesting little radial dependence in the disk fraction. At a given stellar mass, the morphology of a galaxy does not depend strongly on its location within the group.

However, close examination of Figures 4.6 and 4.7 may suggest that the higher overall disk fraction for X-ray groups may be contributed from galaxies located in the outer parts of these groups. In Figure 4.6 a crossover is observed at approximately $0.6r/r_{200}$. Interior to this radius the disk fraction for X-ray groups is lower than for the

optical groups while outside this radius the disk fraction becomes higher and thus the overall higher disk fraction appears to be coming from the galaxies at higher group-centric radii. The results of Figure 4.7 also indicate that the highest disk fraction comes from galaxies found outside of $0.5r_{200}$ in X-ray groups. This is a very subtle effect but something to take note of.

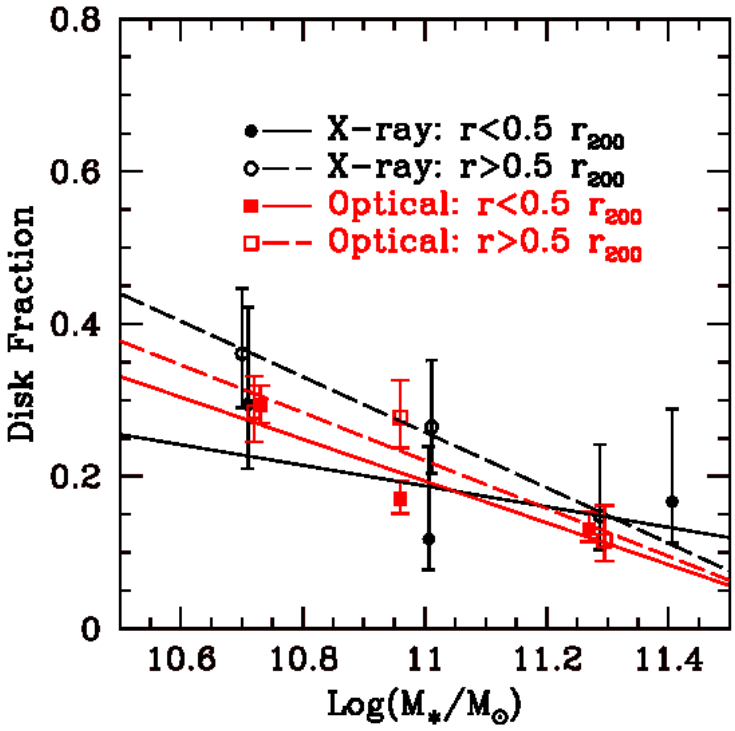

Figure 4.7: Disk fraction as a function of stellar mass for X-ray and optical group galaxies in two group-centric bins. Little dependence of group-centric distance is immediately observed here.

4.4 X-ray Luminosity

As was found in Chapter 3, the passive fractions were different for the X-ray and optical groups. Section 4.1 also showed a difference between the X-ray and optical group galaxies for the disk fractions. This section concentrates on X-ray groups and

searches for any trends in disk fractions with X-ray luminosity.

To delve deeper into possible dependencies on X-ray luminosity, several different cuts were made as described in the following figures. Figure 4.8 shows the disk fraction as a function of X-ray luminosity. The black circles represent the entire sample while the red squares and blue triangles represent the sample divided into low and high stellar mass bins respectively. Lower mass galaxies are more affected by environment (as discussed in Figure 1.4) and thus dividing the sample into these stellar mass bins is useful to see if we can detect a dependence on stellar mass. Overall no trend is observed, especially for the whole sample which shows a very flat disk fraction with X-ray luminosity. The higher mass bin suggests a small slope but a weighted linear least squares fit gives a slope consistent with zero within error. The result does show however that overall lower mass galaxies are typically more disky as they have a higher disk fraction, consistent with the results of Figure 4.1.

The result here is again a little surprising based on the above results from Figure 4.1. Since X-ray group galaxies showed an overall increase in disk fraction compared to optical group galaxies, it may be expected that the disk fraction would increase with X-ray luminosity. However, the lack of a trend with X-ray luminosity is in agreement with the halo mass result of Section 4.2 which also showed a lack of a trend in the disk fraction as a function of halo mass.

To further analyze the X-ray luminosity properties, the upper panel of Figure 4.9 plots the disk fraction as a function of galaxy stellar mass for two X-ray luminosity bins, divided by the median X-ray luminosity of the sample (in units of erg/s). Again, no strong trend is observed with X-ray luminosity as the points overlap at all stellar masses.

Taking the analysis one step further, the lower panel of Figure 4.9 once again plots the disk fraction as a function of galaxy stellar mass but instead of dividing the X-ray luminosities by their median value, the division only includes the extreme least and most X-ray luminous groups. Now, there is suggestion that the more luminous groups

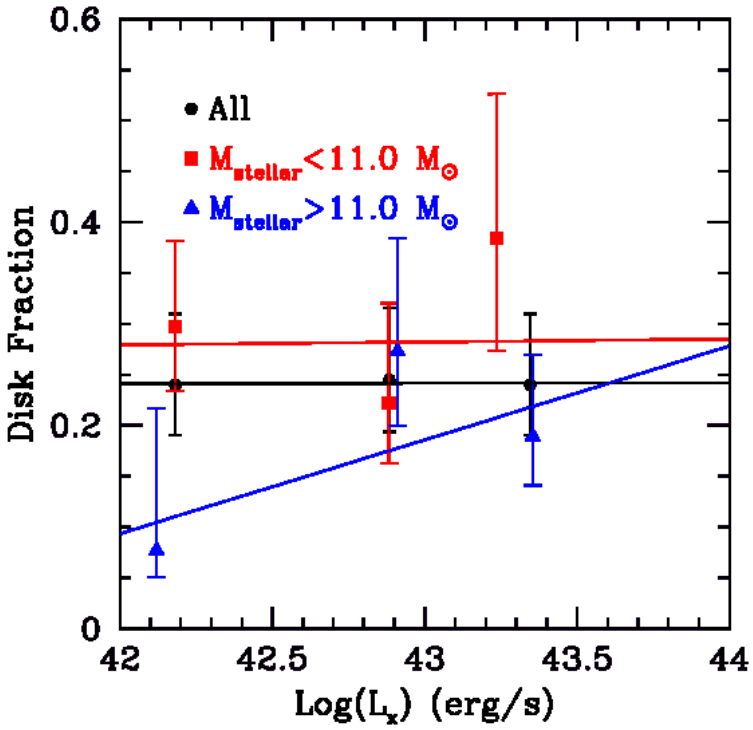

Figure 4.8: Disk fraction as a function of group X-ray luminosity for the entire sample as a whole, as well as for sample subdivided into low and high mass galaxies. No dependence on X-ray luminosity is apparent.

have a higher disk fraction. This supports the result of Figure 4.1 which showed a higher disk fraction for the X-ray groups (with higher X-ray luminosity) than the optical groups but further investigation is needed in order to fully understand the X-ray properties.

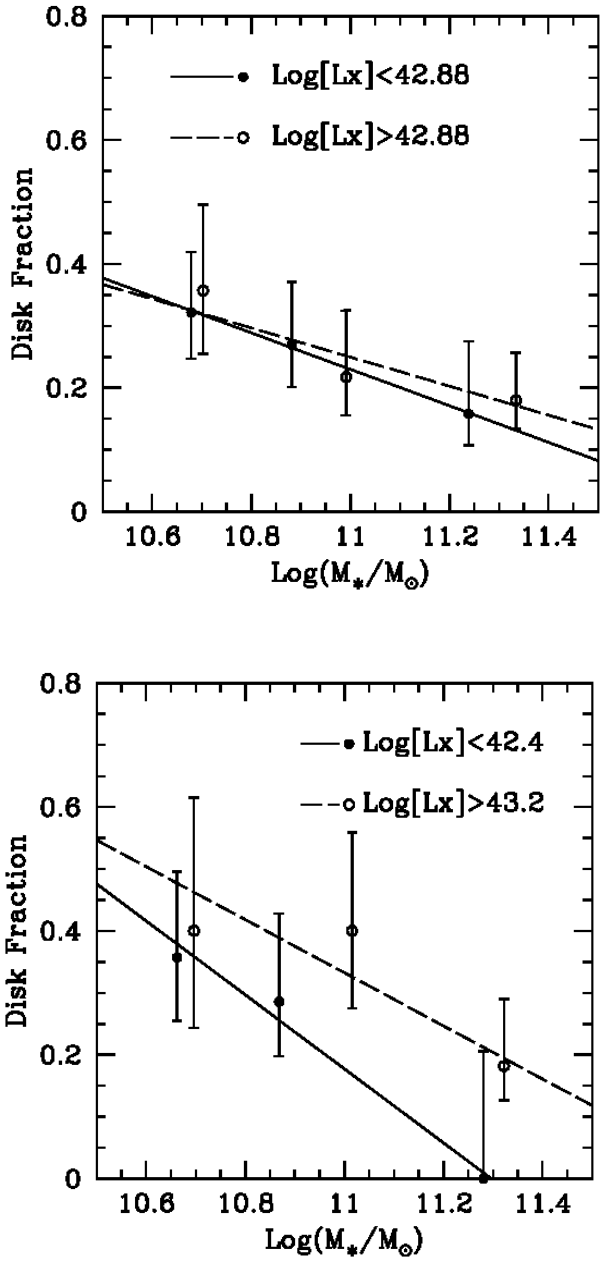

Figure 4.9: Disk fraction as a function of galaxy stellar mass broken into two X-ray luminosity bins divided by their median value (upper panel) and divided to include only the extreme luminosity groups (lower panel). No dependence on X-ray luminosity is seen in the top panel but looking at the extreme value case (bottom) does suggest some differences with the X-ray luminous groups showing a higher disk fraction.

4.5 Redshift

It is known that the number of spiral galaxies increases with redshift (Dressler, 1980). To see if this is evident for the COSMOS sample, Figure 4.10 shows the disk fraction as a function of redshift for field, X-ray and optical group galaxies. The disk fraction increases with redshift in all environments and overall the disk fraction is higher in the field than in groups. Figure 4.10 also suggests that overall the X-ray group galaxies have a higher disk fraction, in agreement with Figure 4.1 although there is some difference at higher redshift. Overall, clear redshift tends are observed for the COSMOS disk fractions with the number of spirals increasing with redshift.

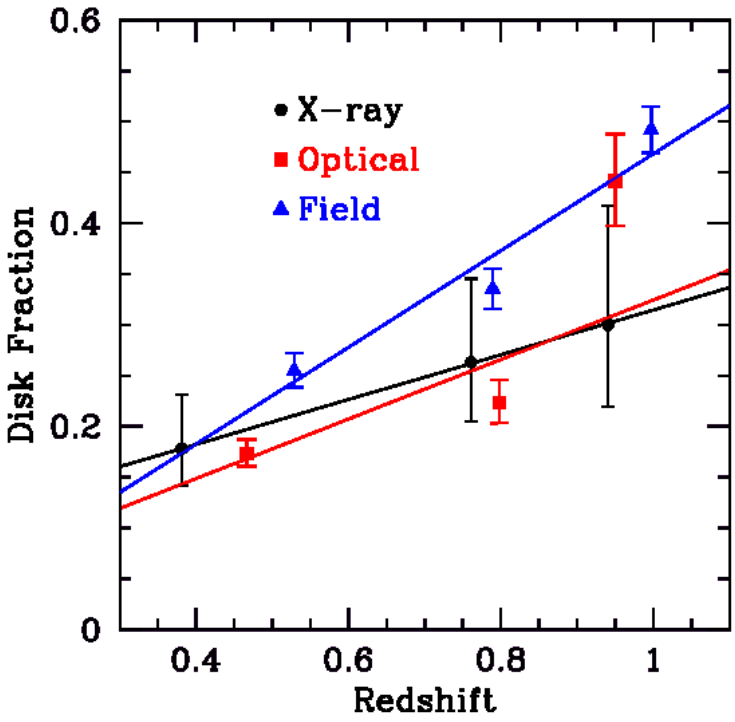

Figure 4.10: Disk fraction as a function of redshift for field, X-ray and optical group galaxies. The disk fraction increases with redshift in all environments and overall the disk fraction is higher in the field than in groups.

4.6 Mass Segregation

As was done for the GEEC sample in Section 3.7, mass segregation was explored for the COSMOS sample. Figure 4.11 shows the mean log stellar mass (in units of solar masses) as a function of group-centric distance for the X-ray and optical groups. In both groups, a slope consistent with zero within error was found suggesting no mass segregation in these groups.

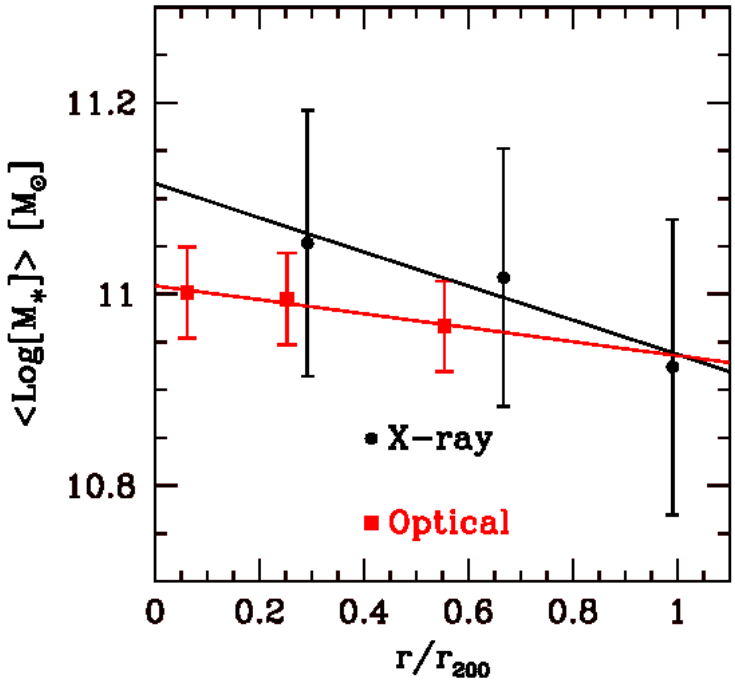

Figure 4.11: Average galaxy stellar mass as a function of group-centric distance for COSMOS. No mass segregation is found as the calculated slopes were consistent with zero within error.

Bibliography

Butcher, H. & Oemler Jr., A., 1978, ApJ, 219, 18

Dressler, A., 1980, ApJ, 236, 315

Dressler, A., Oemler Jr., A., Couch, W. J., et al., 1997, ApJ, 490, 577

George, M. R., Leauthaud, A., Bundy, K., et al., 2011, ApJ, 742, 125

Knobel, C., Lilly, S. J., Iovino, A., et al., 2012, ApJ, 753, 121

Marleau, F. R. & Simard, L., 1998, ApJ, 507, 585

Peng, Y.-j., Lilly, S. J., Kovač, K., et al., 2010, ApJ, 721, 193

Poggianti, B. M., Fasano, G., Bettoni, D., et al., 2009, ApJL, 697, L137

Sargent, M. T., Carollo, C. M., Lilly, S., et al., 2007, ApJS, 172, 434

Scarlata, C., Carollo, C. M., Lilly, S., et al., 2007, ApJS, 172, 406

Chapter 5

Discussion and Conclusions

The general aim of this thesis was to investigate how environment affects galaxy evolution. In particular, how do the properties of galaxies in X-ray and optical groups compare. Star formation rates and galaxy morphologies in each type of group were investigated by calculating passive fractions using the GEEC sample and disk fractions using the COSMOS survey as a function of a number of different parameters including overall environment, group mass, group-centric distance, X-ray luminosity and redshift.

In both the X-ray and optical groups as well as in the field, passive fractions increased while disk fractions decreased with galaxy stellar mass suggesting star-forming galaxies are overall associated with disky galaxies, as expected (Blanton et al., 2003; McGee et al., 2008). However, the rates at which these fractions increased or decreased varied as a function of galaxy stellar mass. To help show this, Table 5.1 summarizes the slopes obtained from weighted linear least squares fits for the passive and disk fractions. Firstly, the table shows that the slopes for the disk fractions are steeper suggesting the disk fraction changes with galaxy stellar mass at a higher rate than the passive fraction. The results also show that the slopes (and also the intercepts, which were also obtained from the weighted linear least squares fit) of the passive fractions for the groups and field overlap within error. On the other hand, the

slopes (and intercepts) of the disk fraction for the field galaxies were different than the group galaxies suggesting a greater difference in the disk fractions between group and field galaxies compared to the passive fractions.

Table 5.1: Slopes for the GEEC passive fractions and COSMOS disk fractions as a function of galaxy stellar mass for galaxies in the field, X-ray and optical groups.

	Field	X-ray	Optical
f_q (Fig. 3.1)	0.3 ± 0.1	0.2 ± 0.2	0.2 ± 0.1
f_D (Fig. 4.1)	-0.66 ± 0.08	-0.3 ± 0.1	-0.29 ± 0.07

It has been shown in Figures 3.1 and 4.1 that the X-ray and optical groups appear to have galaxies with different properties, with the passive and disk fractions both higher for galaxies in the X-ray groups compared to galaxies in the optical groups. This is an interesting result since, as mentioned, disky galaxies typically have more star formation (Blanton et al., 2003; McGee et al., 2008). Thus, the fact that galaxies in X-ray groups appear to be diskier yet have less star formation is a surprising result. However, at first look the results for the passive and disk fractions for galaxies in the optical and X-ray groups are very close, especially evident for the disk fractions where the slopes (and also the intercepts obtained from the weighted linear least squares fit) have very nearly the same values.

To further examine the significance of the difference between the passive and disk fractions of the X-ray and optical groups galaxies, the following procedure was performed. Figures 3.1 and 4.1 both show a strong dependence on stellar mass. Thus, to compare the passive and disk fractions between the X-ray and optical groups this stellar mass trend was removed. This was done by using the first point in each figure as a reference and then removing the stellar mass trend in the other two points by removing the slope from those two points. Once the stellar mass trend was removed, a weighted average of the three points was then calculated. This was done for both the X-ray and optical group galaxy passive fractions and a similar procedure was performed for the disk fractions. For the disk fractions, the weighted averages of the

X-ray and optical group galaxies were 0.35±0.03 and 0.28±0.01 respectively and for the passive fractions the weighted averages after removing the stellar mass trend were 0.64±0.04 and 0.54±0.03 for the X-ray and optical groups galaxies respectively. Both the disk and passive fractions show a greater than 1-σ level of significance difference between the X-ray and optical groups.

Attempts to understand the systematically higher disk fractions for the X-ray group galaxies were made. Spiral galaxies are typically blue and star-forming while elliptical galaxies are typically red and non-star-forming (Blanton et al., 2003). However, as highlighted in the previous paragraph the results of Figures 3.1 and 4.1 of this thesis suggest less star formation in the X-ray groups but also a higher disk-like galaxy fraction in these X-ray groups. To try to gain insight into the difference, an interesting result from the work of Treu et al. (2003) (see their Figure 16) is presented in Figure 5.1. Treu et al. (2003) specifically studied the morphological properties of galaxies in the cluster Cl 0024+16 but their results may be relevant to help explain the disk fraction results found in our groups. They divided the cluster into 38 different regions. The region labeled POS=00 is a central patch of the cluster while the region labeled POS=36 is an over-dense outer patch of the cluster located approximately 1 Mpc from the cluster centre. Figure 5.1 shows the elliptical plus S0-type galaxy fraction and is plotted as a function of local density for galaxies located in the central patch (filled pentagons) and in the over-dense region (open squares). The fraction of elliptical plus S0-type galaxies increases as a function of local density in both patches and there is close agreement in the fractions amongst galaxies near the dense cluster centre and in the over-dense outer region, as the points overlap within error. This suggests that the galaxy morphology is directly related to the local density and thus galaxy properties are strongly determined according to their local environmental conditions. So, this specific result is useful as it illustrates that while in general it is expected see more elliptical-type galaxies near the centres of clusters and more spiral-types farther from the cluster centre where densities typically drop off (Dressler, 1980), sub-clustering

or high density regions that do happen to exist on the cluster outskirts may very well perturb the disks of galaxies and increase the fraction of elliptical plus S0 galaxies.

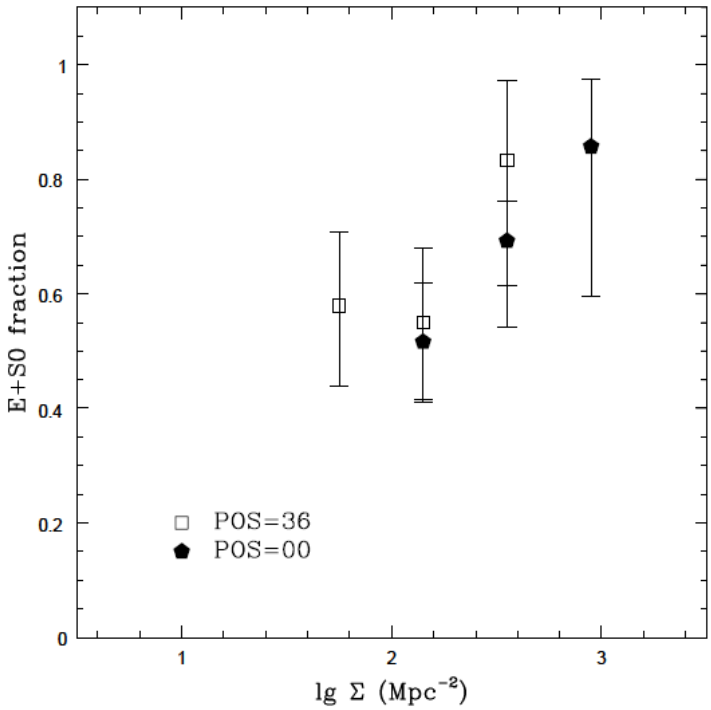

Figure 5.1: A morphology-density relation showing the fraction of elliptical plus S0-type galaxies as a function of local density for galaxies found in a dense inner region (filled pentagons) and an over-dense outer region (open squares, ∼1 Mpc from the cluster centre) for the cluster Cl 0024+16. It shows that an over-dense patch far from the cluster centre can produce a similar elliptical plus S0-type galaxy fraction as is found near the cluster centre indicating that local environmental conditions play an important role in shaping galaxy morphologies and properties. Image credit: Treu et al. (2003) (see their Figure 16). © AAS. Reproduced with permission.

On the group scale then, trying to understand how local galaxy densities of sub-structure or clumps may shape the overall morphologies and properties of the galaxies would be useful. Also, the more evolved X-ray groups may be in the process of accreting a large number of spiral galaxies from the field to the group outskirts which would help explain the higher disk fractions in the X-ray groups. This scenario is somewhat supported by the results of Figures 4.6 and 4.7 which showed the disk frac-

tion was highest in X-ray groups for galaxies away from the group centre (i.e. outside of $0.5r_{200}$). Investigating groups with substructure (as classified in Hou et al., 2012) and/or including lower mass galaxies in the analysis may help to confirm that these trends exist.

To try to quantify if a group mass trend is present, Table 5.2 lists the slopes of the passive and disk fractions for galaxies in X-ray and optical groups as a function of group mass. Both the disk and passive fractions show a slope of zero within error and thus both fractions show no clear dependence in the galaxy properties with group mass is evident.

Table 5.2: Slopes for the GEEC passive fractions and COSMOS disk fractions as a function of halo mass for galaxies in X-ray and optical groups.

	X-ray	Optical
f_q (Fig. 3.3)	-0.07 ± 0.07	0.01 ± 0.07
f_D (Fig. 4.4)	-0.1 ± 0.2	-0.02 ± 0.03

Other work (e.g. Wetzel, Tinker & Conroy, 2012; Giodini et al., 2012) has shown an overall star formation dependence on group mass with less star formation in higher mass groups. The group mass trends for GEEC are not clear in our sample but we have a relatively small sample set. Whether or not disk fractions depend on group or cluster mass (or X-ray luminosity) is also still a matter of debate (Poggianti et al., 2009). Poggianti et al. (2009) find a trend in the disk fractions with cluster mass when using X-ray luminosity as a tracer of halo mass but not when using velocity dispersions as a tracer of halo mass.

The existence of strong radial trends was also not observed in the analysis presented in this thesis although weak trends were observed. Table 5.3 lists the slopes of the passive and disk fractions for the X-ray and optical group galaxies as a function of group-centric distance. The disk fractions suggest an increase in disky galaxies as a function of the distance from the group center as expected from Dressler (1980) but is only significant for the optical group galaxies. The passive fraction trend is

not as significant but does suggest a lower fraction of star-forming galaxies near the group centers which was also observed in Wetzel, Tinker & Conroy (2012) who show less star formation near the group centre. The same trends are observed in both the optical and X-ray groups.

Table 5.3: Slopes for the GEEC passive fractions and COSMOS disk fractions as a function of group-centric distance for galaxies in X-ray and optical groups.

	X-ray	Optical
f_q (Fig. 3.5)	-0.1 ± 0.2	-0.1 ± 0.3
f_D (Fig. 4.6)	0.2 ± 0.2	0.08 ± 0.07

5.1 Summary

To the best of our knowledge this thesis carried out the first in-depth analysis comparing the properties of galaxies in X-ray bright and faint groups, specifically passive fractions from the GEEC sample and disk fractions from the COSMOS survey. Both fractions were calculated as a function of stellar mass, overall environment, group mass, distance from the group centre, redshift and X-ray luminosity. Whether or not there were signatures of mass segregation in our groups was also investigated.

The passive and disk fractions were found to depend most strongly on galaxy stellar mass, redshift and overall environment (i.e. whether or not the galaxy was found in the field or in a group and also whether the galaxy resided in an X-ray or optical group). Both fractions also showed weaker trends with group-centric distance but show no obvious dependence on group halo mass or X-ray luminosity. Trends in star formation rates and morphologies as a function of cluster mass and cluster-centric distance have been studied in detail in clusters (Butcher & Oemler, 1978; Dressler, 1980; Dressler et al., 1997; Treu et al., 2003; Poggianti et al., 2009) but the relationships are still not as clear for groups at this point and remain an active area of research. The main results of this thesis are as follows:

- Field galaxies have a lower passive fraction and a higher disk fraction compared to group galaxies indicating more star formation and more spiral galaxies in the field.

- X-ray group galaxies have higher passive and disk fractions than optical group galaxies. This was a surprising result given that disk-like galaxies are typically star-forming while elliptical-type galaxies typically show less star formation. Removing the stellar mass trend showed that the differences in the passive and disk fractions for the X-ray and optical group galaxies were significant at a greater than 1-σ level. The unexpected trend in the high disk fraction for the X-ray groups needs to be investigated further.

- No obvious trends with group mass are observed. The GEEC sample showed no dependence on group mass while the COSMOS disk fractions also showed no reliance on group mass.

- Weak radial trends are observed. The fraction of disky galaxies increased with group-centric distance (significant for the optical group galaxies but not the X-ray group galaxies) while the fraction of passive galaxies appeared to decrease as a function of group-centric distance (however these results were not significant).

- Passive fractions decreased with increasing redshift while disk fractions increased with increasing redshift confirming higher amounts of star formation and a higher number of disky galaxies at higher redshift in both the field and group samples.

- Neither passive nor disk fractions showed strong trends with X-ray luminosity. The lack of a trend with X-ray luminosity for the X-ray groups is interesting based on the fact that there were differences observed between the X-ray (with higher X-ray luminosities) and optical (with lower X-ray luminosities) group galaxies.

- No significant signs of mass segregation are observed for both the GEEC and COSMOS samples.

5.2 Future Work

A number of interesting trends were observed in this analysis of X-ray and optical groups, but many of the trends are subtle and require further investigation to elucidate.

Many of the results from the GEEC sample were inconclusive, with outlier points and large errors driven by low counting statistics. A first step may then be to complete more surveys and/or make extensions to existing surveys in order to increase the group and galaxy sample size (in effect decreasing the errors in the results and helping better discern any trends in the data). Another way to increase the statistics could be to apply completeness weights (Balogh et al., 2009; Connelly et al., 2012) to pre-existing surveys such as GEEC which would allow analysis to lower stellar masses in effect creating a larger sample size and decreasing errors.

Furthermore, in addition to completeness weights for the GEEC sample, further follow up of the sample would be very useful. Spectroscopic redshift data is currently available to a redshift of approximately 1 for galaxies in the GEEC X-ray selected group sample. However, star formation rates are only available up to a redshift of approximately 0.6. Extending the star formation data to a redshift of 1 or higher and doing the same for galaxies in the optically selected groups (as there are no optically selected GEEC groups at z>0.6) would allow for a fuller comparison to the COSMOS data which extended to a redshift of approximately 1.

There are several other useful extensions which could be made to further compare and utilize both GEEC and COSMOS. All the trends observed for COSMOS in this thesis used a conservative stellar mass cut of $10^{10.6} M_{\odot}$. Looking at the lower mass galaxies would be useful. In addition, studying morphology data for GEEC groups

(which is currently available for a small number of GEEC optical group galaxies) and conversely studying star formation rates for the COSMOS data (a work currently in progress) would also allow for a more robust comparison between the two surveys. Comparing to other large low redshift surveys such as the SDSS (e.g. Wang et al., 2011; McGee et al., 2011; Yang et al., 2007) would also allow for a better investigation of the trends. Ideally passive and disk fractions should be measured for the same set of galaxies with the same completeness limits.

As was shown in this thesis, the properties of galaxies such as their star formation rates and morphologies depend strongly on stellar mass and redshift. Trends with environmental properties such as group-centric distance and group mass appear to be much weaker and are thus much more challenging to study. It is critical to carefully control for stellar mass and redshift when investigating environmental trends. An alternative to the analysis presented here is to match each group galaxy with a control field galaxy with the same stellar mass and redshift. Hence, in this case it would be known that the stellar mass and redshift properties of the galaxies are very similar and can be compared more closely without having to consider the effects of a stellar mass or redshift discrepancy. On a similar note to matching individual galaxies, looking at the properties of component galaxies from individual groups in detail (instead of all groups collectively at once as was done in this thesis) would be useful.

Looking at groups with and without substructure (as classified in Hou et al. (2012), for example) would help in understanding the overall dynamical complexity of the groups and help determine if the optical groups that have substructure and possibly high local galaxy densities contribute to the lower disk fractions (as discussed in Fig. 5.1) and/or are typically less evolved than the X-ray counterparts.

In addition, studying the colours of the group galaxies (Balogh et al., 2009) and relating the colours to the passive and disk fractions would help to further understand the properties of group galaxies. The relationships between star formation, galaxy morphology and colour has been studied extensively in clusters (e.g. Butcher

& Oemler, 1978; Nilo Castellón et al., 2014; Cohen et al., 2014; Dressler et al., 1997) but work is still in progress on the group scale. Red galaxies tend to have lower star formation rates than bluer galaxies and so the colours of galaxies can be used as a tracer for star formation. Comparing colours to morphology would also add to the picture. If a large number of blue elliptical galaxies were confirmed in the COSMOS optical group galaxy sample or a large number of red spiral galaxies in the X-ray group galaxy sample for example, it could help explain the higher passive and disk fractions found in the X-ray groups. Understanding the relationships not only between star formation rates and morphology but also between colour and morphology is very important to fully understand the properties of galaxies in groups.

Bibliography

Balogh, M. L., McGee, S. L., Wilman, D. J., et al., 2009, MNRAS, 398, 754

Blanton, M. R., Hogg, D. W., Bahcall, N. A., et al., 2003, ApJ, 594, 186

Butcher, H. & Oemler Jr., A., 1978, ApJ, 219, 18

Cohen, S. A., Hickox, R. C., Wegner, G. A., et al., 2014, ApJ, 783, 136

Connelly, J. L., Wilman, D. J., Finoguenov, A., et al., 2012, ApJ, 756, 139

Dressler, A., 1980, ApJ, 236, 315

Dressler, A., Oemler Jr., A., Couch, W. J., et al., 1997, ApJ, 490, 577

Finoguenov, A., Guzzo, L., Hasinger, G., et al., 2007, ApJS, 172, 182

Giodini, S., Finoguenov, A., Pierini, D., et al., 2012, A&A, 538, A104

Hou, A., Parker, L. C., Wilman, D. J., et al. 2012, MNRAS, 421, 3594

McGee, S. L., Balogh, M. L., Henderson, R. D. E., et al., 2008, MNRAS, 387, 1605

McGee, S. L., Balogh, M. L., Wilman, D. J., et al., 2011, MNRAS, 413, 996

Nilo Castellón, J. L., Alonso, M. V., García Lambas, D., et al., 2014, MNRAS, 437, 2607

Poggianti, B. M., Fasano, G., Bettoni, D., et al., 2009, ApJL, 697, L137

Rawle, T. D., Altieri, B., Egami, E., et al., 2014, MNRAS, 442, 196

Treu, T., Ellis, R. S., Kneib, J-P., et al., 2003, ApJ, 591, 53

Urquhart, S. A., Willis, J. P., Hoekstra, H., et al., 2010, MNRAS, 406, 368

Wang, L., Yang, X., Luo, W., et al., 2011, arXiv:1110.1987

Wetzel, A. R., Tinker, J. L. & Conroy, C., 2012, MNRAS, 424, 232

Yang, X., Mo, H. J., van den Bosch, F. C., et al., 2007, ApJ, 671, 153

Ziparo, F., Popesso, P., Biviano, A., et al., 2013, MNRAS, 434, 3089